

When the anomalistic, draconitic and sidereal orbital periods do not coincide: the impact of post-Keplerian perturbing accelerations

Lorenzo Iorio¹

¹Ministero dell' Istruzione e del Merito. Viale Unità di Italia 68, I-70125, Bari (BA), Italy

Abstract

In a purely Keplerian picture, the anomalistic, draconitic and sidereal orbital periods of a test particle orbiting a massive body coincide with each other. Such a degeneracy is removed when a post-Keplerian perturbing acceleration enters the equations of motion yielding generally different corrections to the Keplerian period for the three aforementioned characteristic orbital timescales. They are analytically worked out in the case of the accelerations induced by the general relativistic post-Newtonian gravitoelectromagnetic fields and, to the Newtonian level, by the oblateness of the central body as well. The resulting expressions hold for completely general orbital configurations and spatial orientations of the spin axis of the primary. Astronomical systems characterized by extremely accurate measurements of the orbital periods like, e.g., transiting exoplanets and binary pulsars, may offer potentially viable scenarios for measuring such post-Keplerian features of motion, at least in principle. As an example, the sidereal period of the brown dwarf WD1032 + 011 b is currently known with an uncertainty as small as $\approx 10^{-5}$ s, while its predicted post-Newtonian gravitoelectric correction amounts to 0.07 s; however, the accuracy with which the Keplerian period can be calculated is just 572 s. For the double pulsar PSR J0737–3039, the largest relativistic correction to the anomalistic period amounts to a few tenths of a second, given a measurement error of such a characteristic orbital timescale as small as $\approx 10^{-6}$ s. On the other hand, the Keplerian term can be currently calculated just to a ≈ 9 s accuracy. In principle, measuring at least two of the three characteristic orbital periods for the same system independently would allow to cancel out their common Keplerian component provided that their difference is taken.

Keywords: Classical general relativity; Experimental studies of gravity; Experimental tests of gravitational theories; Time and frequency; Extrasolar planetary systems

1. Introduction

From a theoretical point of view, various time intervals T characterizing different cyclic patterns of the orbital motion of a two-body gravitationally bound system can be defined when, in addition to the dominant Newtonian inverse-square acceleration, also a much smaller, post-Keplerian¹ (pK) one A acts on a satellite. Such characteristic orbital timescales are the amounts of time elapsed between two successive passages of the latter at some directions which, in a purely Keplerian scenario, are all fixed; in this case, all such periods coincide with the Keplerian one T_K . Instead, a pK perturbation breaks such a degeneracy, and the aforementioned temporal intervals generally differ one from each other.

Aim of the present work is to analytically work out the corrections ΔT to T_K induced by the gravitoelectromagnetic accelerations arising within the General Theory of Relativity (GTR) to the first post-Newtonian (1pN) order (Mashhoon 2001, 2007). Furthermore, also the impact of the oblateness of the central body (Capderou 2005) is worked out to the Newtonian level. In all the aforementioned three cases, the anomalistic, draconitic and sidereal periods are considered. The resulting expressions turn out to be valid for completely general orbital shapes and inclinations, and for arbitrary orientations of the primary's spin axis in space. For analogous calculation restricted to some particular orbital geometries, see Iorio (2016). In addition to the traditional quantities usually adopted like, e.g., the time-honoured pericentre precession, the orbital periods, if directly measured, may offer, in principle, further ways to test GTR and other models of gravity as well.

lorenzo.iorio@libero.it

¹ Here, by “post-Keplerian” one means dynamical features arising from any acceleration, Newtonian or not, different from the simple Newtonian inverse-square one. Then, in this specific sense, the classical acceleration due to, say, the primary's oblateness J_2 has to be meant as pK.

In recent years, exoplanets (Mason 2008; Seager 2011; Kitchin 2012; Deeg and Belmonte 2018; Perryman 2018) have been attracting a growing interest as possible tools to test GTR and modified models of gravity (Adams and Laughlin 2006c,a,b; Iorio 2006; Jordán and Bakos 2008; Pál and Kocsis 2008; Jordán and Bakos 2009; Ragozzine and Wolf 2009; Iorio and Ruggiero 2010; Damiani and Lanza 2011; Fukui et al. 2011; Iorio 2011a,b; Eibe et al. 2012; Kane et al. 2012; Li 2012; Zhao and Xie 2013; Xie and Deng 2014; Vargas dos Santos and Mota 2017; Blanchet et al. 2019; Marzari and Nagasawa 2019; Ruggiero and Iorio 2020; Antoniciello et al. 2021; Gou et al. 2021; Kozak and Wojnar 2021). For comprehensive overviews of tests of GTR, see, e.g., Will (2014, 2018); Will and Yunes (2020), and references therein. The results presented here may have an impact on, e.g., just exoplanetary studies since the accuracy in measuring the orbital periods of some transiting planets is currently quite remarkable. Even better is the accuracy with which the anomalistic periods of binary pulsars are usually measured.

The paper is organized as follows. In Section 2, the pK accelerations treated are reviewed: the 1pN gravitoelectric (Section 2.1) and gravitomagnetic (Section 2.2), and the Newtonian quadrupolar one (Section 2.3). Section 3 is devoted to the anomalistic period; the general calculational scheme is outlined in Section 3.1, while the 1pN and the quadrupolar corrections are worked out in Sections 3.2 to 3.4. The draconitic period is dealt with in Section 4; Section 4.1 shows how to calculate it, while the 1pN and the quadrupolar corrections are the subjects of Sections 4.2 to 4.4. The sidereal period is investigated in Section 5; the calculational approach is explained in Section 5.1, while the 1pN and the quadrupolar corrections are calculated in Sections 5.2 to 5.4. In Section 6, a numerical evaluation of the 1pN gravitoelectric effect for a transiting exoplanet and the double pulsar whose orbital periods are accurately measured is offered. Section 7 summarizes the findings and offers conclusions.

2. The pK accelerations

Here, a brief summary of some key concepts of celestial mechanics, needed to follow the rest of the paper profitably, is offered (Brouwer and Clemence 1961; Soffel 1989; Brumberg 1991; Bertotti et al. 2003; Roy 2005; Kopeikin et al. 2011; Poisson and Will 2014; Soffel and Han 2019).

If \mathbf{A} is an arbitrary pK perturbing acceleration, generally depending on the position and velocity vectors \mathbf{r} and \mathbf{v} of the orbiter, calculating its effects on the orbital path of the latter requires the knowledge of its radial, transverse and normal components A_r , A_τ and A_h . They are the projections $\mathbf{A} \cdot \hat{\mathbf{r}}$, $\mathbf{A} \cdot \hat{\boldsymbol{\tau}}$ and $\mathbf{A} \cdot \hat{\mathbf{h}}$ of \mathbf{A} onto the co-moving radial, transverse and normal unit vectors

$$\hat{\mathbf{r}} = \{\cos \Omega \cos u - \cos I \sin \Omega \sin u, \sin \Omega \cos u + \cos I \cos \Omega \sin u, \sin I \sin u\}, \quad (1)$$

$$\hat{\boldsymbol{\tau}} = \{-\cos \Omega \sin u - \cos I \sin \Omega \cos u, -\sin \Omega \sin u + \cos I \cos \Omega \cos u, \sin I \cos u\}, \quad (2)$$

$$\hat{\mathbf{h}} = \{\sin I \sin \Omega, -\sin I \cos \Omega, \cos I\}. \quad (3)$$

In Equations (1)–(3), I is the inclination of the orbital plane to the reference plane of the coordinate system adopted, Ω is the longitude of the ascending node², and u is the argument of latitude³ defined as

$$u := \omega + f. \quad (4)$$

In Equation (4), ω is the argument of pericentre⁴, and f is the true anomaly⁵. The normal unit vector, given by Equation (3), is aligned with the orbital angular momentum; Equations (1)–(3) are connected at each instant of time by the relation

$$\hat{\mathbf{h}} \times \hat{\mathbf{r}} = \hat{\boldsymbol{\tau}}. \quad (5)$$

Then, A_r , A_τ and A_h are to be evaluated onto the Keplerian ellipse, assumed as unperturbed reference trajectory; it is given by

$$r = \frac{p}{1 + e \cos f}. \quad (6)$$

In Equation (6), e is the eccentricity⁶, and

$$p := a(1 - e^2) \quad (7)$$

² It is an angle counted in the reference plane from the reference x direction to the line of nodes, which is the intersection of the orbital plane with the fundamental one.

³ It is a time-dependent angle reckoned in the orbital plane from the line of nodes to the instantaneous position of the test particle moving along the ellipse.

⁴ It is an angle reckoned in the orbital plane from the line of nodes to the position of the pericentre on the line of apsides.

⁵ It is a time-dependent angle counted in the orbital plane from the position of the pericentre on the line of apsides to the instantaneous position of the test particle moving along the ellipse. Thus, it is often used as fast variable of integration when the average over one orbital period of some relevant quantity instantaneously varying during the satellite's orbital revolution is calculated.

⁶ It fixes the shape of the ellipse; $0 \leq e < 1$, where $e = 0$ corresponds to a circular orbit.

is the orbit's semilatus rectum; a is the semimajor axis⁷. The position and velocity vectors, generally entering the analytical expression of \mathbf{A} , can be conveniently expressed as

$$\mathbf{r} = r(\hat{\mathbf{l}} \cos u + \hat{\mathbf{m}} \sin u), \quad (8)$$

$$\mathbf{v} = \sqrt{\frac{\mu}{p}} \left[-\hat{\mathbf{l}}(e \sin \omega + \sin u) + \hat{\mathbf{m}}(e \cos \omega + \cos u) \right]. \quad (9)$$

In Equations (8)–(9), r is given by Equation (6), while

$$\hat{\mathbf{l}} := \{\cos \Omega, \sin \Omega, 0\}, \quad (10)$$

$$\hat{\mathbf{m}} := \{-\cos I \sin \Omega, \cos I \cos \Omega, \sin I\} \quad (11)$$

are two unit vectors lying in the orbital plane; $\hat{\mathbf{l}}$ is directed along the line of nodes, while $\hat{\mathbf{m}}$ is perpendicular to $\hat{\mathbf{l}}$ in such a way that

$$\hat{\mathbf{l}} \times \hat{\mathbf{m}} = \hat{\mathbf{h}}. \quad (12)$$

Finally,

$$\mu := GM \quad (13)$$

entering Equation (9) is the standard gravitational parameter of the primary; M is its mass, and G is the Newtonian constant of gravitation.

2.1. The 1pN gravitoelectric acceleration

In the case of a binary system made of two non-rotating bodies A and B of finite masses M_A and M_B , the 1pN gravitoelectric acceleration is (see, e.g., [Damour and Deruelle 1985](#), Equation (2.5), p. 111; [Soffel 1989](#), Equation (A2.6), p. 166; [Brumberg 1991](#), Equation (4.4.28), p. 154; [Soffel and Han 2019](#), Equation (10.3.7), p. 381; [Poisson and Will 2014](#), Equation (10.1), p. 482)

$$\mathbf{A}^{1pN} = \frac{\mu_b}{c^2 r^2} \left\{ \left[(4 + 2\nu) \frac{\mu_b}{r} + \frac{3}{2} \nu v_r^2 - (1 - 3\nu) v^2 \right] \hat{\mathbf{r}} + (4 - 2\nu) v_r \mathbf{v} \right\}. \quad (14)$$

In Equation (14), c is the speed of light in vacuum, and

$$\mu_b := GM_b \quad (15)$$

is the standard gravitational parameter of the binary whose total mass is

$$M_b := M_A + M_B. \quad (16)$$

Moreover,

$$\nu := \frac{M_A M_B}{M_b^2} \quad (17)$$

is the binary's symmetric mass ratio ranging from 0 if one of the two bodies can be considered as a test particle to $1/4 = 0.25$ if both bodies have the same mass, \mathbf{r} is the position vector of one body with respect to the other one, $\hat{\mathbf{r}}$ is its unit vector, r is its magnitude giving the relative distance between the two bodies, \mathbf{v} is the relative velocity between them, whose magnitude is v , while

$$v_r := \mathbf{v} \cdot \hat{\mathbf{r}} \quad (18)$$

is the projection of the relative velocity onto the position unit vector. By using Equations (1)–(4) and Equations (6)–(11), the radial, transverse and normal components A_r^{1pN} , A_t^{1pN} , A_h^{1pN} of Equation (14) turn out to be

$$A_r^{1pN} = \frac{\mu_b^2 (1 + e \cos f)^2}{4c^2 a^3 (1 - e^2)^3} \left[e^2 (4 - 13\nu) - 4(-3 + \nu) + 8e(1 - 2\nu) \cos f + e^2 (-8 + \nu) \cos 2f \right], \quad (19)$$

⁷ It determines the size of the ellipse

$$A_r^{1\text{pN}} = \frac{2e\mu_b^2 (1 + e \cos f)^3 (2 - \nu) \sin f}{c^2 a^3 (1 - e^2)^3}, \quad (20)$$

$$A_h^{1\text{pN}} = 0. \quad (21)$$

Equations (19)–(21) agree with, e.g., Equations (A2.77a)–(A2.77c), calculated with GTR, by [Soffel \(1989, p. 178\)](#).

2.2. The 1pN gravitomagnetic Lense–Thirring acceleration

The 1pN gravitomagnetic Lense–Thirring (LT) acceleration due to the angular momentum \mathbf{J} of a massive primary, is, for an arbitrary orientation of the latter, ([Soffel 1989](#); [Huang et al. 1990](#); [Damour et al. 1994](#); [Petit and Luzum 2010](#); [Poisson and Will 2014](#); [Soffel and Han 2019](#))

$$\mathbf{A}^{\text{LT}} = \frac{2GJ}{c^2 r^3} \left[3 (\hat{\mathbf{J}} \cdot \hat{\mathbf{r}}) \hat{\mathbf{r}} \times \boldsymbol{\nu} + \boldsymbol{\nu} \times \hat{\mathbf{J}} \right]. \quad (22)$$

In Equation (22), $\hat{\mathbf{J}}$ is the primary's spin axis which can be parameterized as, e.g.,

$$\hat{J}_x = \cos \alpha_J \cos \delta_J, \quad (23)$$

$$\hat{J}_y = \sin \alpha_J \cos \delta_J, \quad (24)$$

$$\hat{J}_z = \sin \delta_J, \quad (25)$$

where α_J and δ_J are its longitude and latitude angles in some coordinate system. For a generalization of Equation (22) to a two–body system with comparable masses and spins, see, e.g., [Kidder \(1995, Equation \(2.2.c\)\)](#), and [Soffel \(1989\)](#). Basically, if \mathbf{J}_A and \mathbf{J}_B are the spin angular momenta of the extended bodies A and B, \mathbf{J} has to be replaced in Equation (22) and in all the following Equations with

$$\mathbf{S}_b := \left(1 + \frac{3 M_B}{4 M_A} \right) \mathbf{J}_A + \left(1 + \frac{3 M_A}{4 M_B} \right) \mathbf{J}_B \quad (26)$$

It is useful to define the following quantities:

$$\mathbb{J}l := \hat{\mathbf{J}} \cdot \hat{\mathbf{l}}, \quad (27)$$

$$\mathbb{J}m := \hat{\mathbf{J}} \cdot \hat{\mathbf{m}}, \quad (28)$$

$$\mathbb{J}h := \hat{\mathbf{J}} \cdot \hat{\mathbf{h}}. \quad (29)$$

By means of Equations (1)–(4), Equations (6)–(9) and Equations (27)–(29), the radial, transverse and normal components A_r^{LT} , A_τ^{LT} , A_h^{LT} of Equation (22) can be written as

$$A_r^{\text{LT}} = \frac{2n_K G J (1 + e \cos f)^4 \mathbb{J}h}{c^2 a^2 (1 - e^2)^{7/2}}, \quad (30)$$

$$A_\tau^{\text{LT}} = -\frac{2en_K G J (1 + e \cos f)^3 \sin f \mathbb{J}h}{c^2 a^2 (1 - e^2)^{7/2}}, \quad (31)$$

$$A_h^{\text{LT}} = -\frac{2n_K G J (1 + e \cos f)^3}{c^2 a^2 (1 - e^2)^{7/2}} \left\{ [e \cos \omega - (2 + 3e \cos f) \cos u] \mathbb{J}l - \frac{1}{2} [e \sin \omega + 4 \sin u + 3e \sin (2f + \omega)] \mathbb{J}m \right\}, \quad (32)$$

where

$$n_K := \sqrt{\frac{\mu}{a^3}} = \frac{2\pi}{T_K} \quad (33)$$

is the Keplerian mean motion.

2.3. The Newtonian quadrupolar acceleration

The pK acceleration induced by the first even zonal harmonic coefficient J_2 of the multipolar expansion of the exterior Newtonian gravitational potential of a massive primary endowed with axial symmetry is

$$\mathbf{A}^{J_2} = \frac{3\mu J_2 R_e^2}{2r^4} \left\{ \left[5 (\hat{\mathbf{J}} \cdot \hat{\mathbf{r}})^2 - 1 \right] \hat{\mathbf{r}} - 2 (\hat{\mathbf{J}} \cdot \hat{\mathbf{r}}) \hat{\mathbf{J}} \right\}, \quad (34)$$

where R_e is the body's equatorial radius.

By defining

$$\widehat{T}_1 := 1, \quad (35)$$

$$\widehat{T}_2 := \mathbb{J}^2 + \mathbb{J}m^2, \quad (36)$$

$$\widehat{T}_3 := \mathbb{J}^2 - \mathbb{J}m^2, \quad (37)$$

$$\widehat{T}_4 := \mathbb{J}h \mathbb{J}l, \quad (38)$$

$$\widehat{T}_5 := \mathbb{J}h \mathbb{J}m, \quad (39)$$

$$\widehat{T}_6 := \mathbb{J}l \mathbb{J}m, \quad (40)$$

and by means of Equations (1)–(4) and Equations (6)–(8), the radial, transverse and normal components $A_r^{J_2}$, $A_\tau^{J_2}$, $A_h^{J_2}$ of Equation (34) can be cast into the form

$$A_r^{J_2} = \frac{3\mu J_2 R_e^2 (1 + e \cos f)^4}{2a^4 (1 - e^2)^4} \left[-\widehat{T}_1 + 3 \left(\frac{\widehat{T}_2}{2} + \frac{\widehat{T}_3 \cos 2u}{2} + \widehat{T}_6 \sin 2u \right) \right], \quad (41)$$

$$A_\tau^{J_2} = \frac{3\mu J_2 R_e^2 (1 + e \cos f)^4}{a^4 (1 - e^2)^4} \left(\frac{\widehat{T}_3 \sin 2u}{2} - \widehat{T}_6 \cos 2u \right), \quad (42)$$

$$A_h^{J_2} = -\frac{3\mu J_2 R_e^2 (1 + e \cos f)^4}{a^4 (1 - e^2)^4} (\widehat{T}_4 \cos u + \widehat{T}_5 \sin u). \quad (43)$$

If both bodies A and B are extended and axisymmetric, Equation (34) becomes (Barker and O'Connell 1975)

$$\mathbf{A}^{J_2} = \frac{3\mu_b}{2r^4} \mathcal{F}_{AB}, \quad (44)$$

where

$$\mathcal{F}_{AB} := J_2^A R_e^{A2} \left\{ \left[5 (\hat{\mathbf{J}}^A \cdot \hat{\mathbf{r}})^2 - 1 \right] \hat{\mathbf{r}} - 2 (\hat{\mathbf{J}}^A \cdot \hat{\mathbf{r}}) \hat{\mathbf{J}}^A \right\} + J_2^B R_e^{B2} \left\{ \left[5 (\hat{\mathbf{J}}^B \cdot \hat{\mathbf{r}})^2 - 1 \right] \hat{\mathbf{r}} - 2 (\hat{\mathbf{J}}^B \cdot \hat{\mathbf{r}}) \hat{\mathbf{J}}^B \right\}, \quad (45)$$

and r and $\hat{\mathbf{r}}$ entering Equations (44)–(45) refer to the relative orbit.

3. The apsidal period

3.1. General calculational scheme

The anomalistic period T_{ano} is defined as the time interval between two successive instants when the real position of the test particle coincides with the pericentre position on the corresponding orbit. It can be calculated as (Zhongolovich 1960; Mioc and Radu 1979; Iorio 2016)

$$T_{\text{ano}} = T_K + \Delta T_{\text{ano}} = \int_0^{2\pi} \left(\frac{dt}{df} \right) df, \quad (46)$$

where dt/df , when a pK acceleration A is present, is given by

$$\frac{dt}{df} \simeq \frac{r^2}{\sqrt{\mu p}} \left[1 + \frac{r^2}{\sqrt{\mu p}} \left(\frac{d\omega}{dt} + \cos I \frac{d\Omega}{dt} \right) \right], \quad (47)$$

since (Egorov 1958; Taratynova 1959; Mioc and Radu 1979; Brumberg 1991; Bertotti et al. 2003; Poisson and Will 2014)

$$\frac{df}{dt} = \frac{\sqrt{\mu p}}{r^2} \left[1 - \frac{r^2}{\sqrt{\mu p}} \left(\frac{d\omega}{dt} + \cos I \frac{d\Omega}{dt} \right) \right]. \quad (48)$$

The true anomaly f enters Equation (46) as fast variable of integration just because the line of apsides is involved in the definition of anomalistic period. In order to obtain the full correction ΔT_{ano} of the order of A to the Keplerian orbital period, the contribution of the second term of Equation (47) to Equation (46) is not enough. Indeed, also the partial derivatives of the Keplerian term of Equation (47)

$$\left. \frac{dt}{df} \right|_{\text{K}} = \frac{r^2}{\sqrt{\mu p}} \quad (49)$$

with respect to a and e , multiplied by the finite variations $\Delta a(f)$, $\Delta e(f)$ of the same orbital elements, have to be taken; in this way, one fully accounts for the fact that the Keplerian orbital elements vary instantaneously as the satellite goes along its trajectory. Thus, it is finally obtained

$$\Delta T_{\text{ano}} = \int_0^{2\pi} \left\{ \frac{3}{2} \sqrt{\frac{a(1-e^2)^3}{\mu}} \frac{\Delta a(f)}{(1+e \cos f)^2} - \sqrt{\frac{a^3(1-e^2)}{\mu}} \frac{[3e + (2+e^2) \cos f]}{(1+e \cos f)^3} \Delta e(f) + \frac{r^4}{\mu p} \left(\frac{d\omega}{dt} + \cos I \frac{d\Omega}{dt} \right) \right\}_{\text{K}} df. \quad (50)$$

The suffix K in Equation (50) means that the content of the curly brackets to which it is appended has to be evaluated onto the unperturbed Keplerian ellipse given by Equation (6). Furthermore, the instantaneous shifts $\Delta \kappa(f)$ of $\kappa = a, e$ are calculated, to the first order in the perturbing pK acceleration A , as

$$\Delta \kappa(f) = \int_{f_0}^f \frac{d\kappa}{df'} df' = \int_{f_0}^f \frac{d\kappa}{dt} \frac{dt}{df'} df', \quad (51)$$

where $d\kappa/dt$ are the Gauss equations for the variations of $\kappa = a, e$ (Brouwer and Clemence 1961; Soffel 1989; Brumberg 1991; Bertotti et al. 2003; Roy 2005; Kopeikin et al. 2011; Poisson and Will 2014; Soffel and Han 2019)

$$\frac{da}{dt} = \frac{2}{n_{\text{K}} \sqrt{1-e^2}} \left[e A_r \sin f + \left(\frac{p}{r} \right) A_{\tau} \right], \quad (52)$$

$$\frac{de}{dt} = \frac{\sqrt{1-e^2}}{n_{\text{K}} a} \left\{ A_r \sin f + A_{\tau} \left[\cos f + \frac{1}{e} \left(1 - \frac{r}{a} \right) \right] \right\}. \quad (53)$$

Finally, $d\Omega/dt$ and $d\omega/dt$ entering the third term of Equation (50) are the Gauss equations for the variations of the longitude of the ascending node and the argument of pericentre, respectively, given by (Brouwer and Clemence 1961; Soffel 1989; Brumberg 1991; Bertotti et al. 2003; Roy 2005; Kopeikin et al. 2011; Poisson and Will 2014; Soffel and Han 2019)

$$\frac{d\Omega}{dt} = \frac{1}{n_{\text{K}} a \sin I \sqrt{1-e^2}} A_h \left(\frac{r}{a} \right) \sin u, \quad (54)$$

$$\frac{d\omega}{dt} = \frac{\sqrt{1-e^2}}{n_{\text{K}} a e} \left[-A_r \cos f + A_{\tau} \left(1 + \frac{r}{p} \right) \sin f \right] - \cos I \frac{d\Omega}{dt}. \quad (55)$$

In (Iorio 2016), a variant of the above calculation can be found; in Equation (49), p is adopted as independent variable along with the eccentricity e , and simpler expressions for the partial derivatives of Equation (49) are obtained. The resulting expressions for calculating ΔT_{ano} turns out to be

$$\Delta T_{\text{ano}} = \int_0^{2\pi} \left\{ \frac{3}{2} \sqrt{\frac{p}{\mu}} \frac{\Delta p(f)}{(1+e \cos f)^2} - 2 \sqrt{\frac{p^3}{\mu}} \frac{\cos f \Delta e(f)}{(1+e \cos f)^3} + \frac{r^4}{\mu p} \left(\frac{d\omega}{dt} + \cos I \frac{d\Omega}{dt} \right) \right\} df. \quad (56)$$

The first-order variation $\Delta p(f)$ of the semilatus rectum can be calculated from (Taratynova 1959; Mioc and Radu 1979)

$$\frac{dp}{df} = \frac{2r^3 A_\tau}{\mu}. \quad (57)$$

In the end, both Equation (50) and Equation (56) give the same result.

The presence or not of the pK anomalistic correction ΔT_{ano} to the orbital period can be intuitively explained as follows. According to

$$\eta = n_{\text{K}} (t_0 - t_p), \quad (58)$$

where η is the mean anomaly at epoch, t_0 is the initial epoch and t_p is the time of passage at pericentre, the rate of change of the η is proportional to the opposite of the pace of variation of t_p . Thus, should η increase, the crossing of the pericentre position would be anticipated with respect to the Keplerian case since t_p would decrease, and vice versa. In this case, the variation of η would result in an orbit-by-orbit advance or delay of the passages at the pericentre. As it will be shown, while the 1pN gravitoelectric acceleration of Equation (14) does induce a negative rate of η , the gravitomagnetic LT one of Equation (22) leaves the mean anomaly at epoch unchanged. Furthermore, several modified models of gravity, inducing radial pK accelerations dependent only on r , secularly change both ω and η . Also the Newtonian acceleration raised by the primary's oblateness J_2 affects, among other things, also η .

3.2. The 1pN gravitoelectric correction

The 1pN anomalistic period can be calculated by means of Equations (19)–(21) as explained in Section 3.1. It turns out to be

$$T_{\text{ano}}^{1\text{pN}} = T_{\text{K}} + \Delta T_{\text{ano}}^{1\text{pN}}, \quad (59)$$

with

$$\begin{aligned} \Delta T_{\text{ano}}^{1\text{pN}} = & \frac{\pi \sqrt{\mu_b a}}{2c^2 (1-e^2)^2} \left(36 + e^2 (42 - 38\nu) + 2e^4 (6 - 7\nu) - 8\nu + 3e \left[[28 + 3e^2 (4 - 5\nu) - 12\nu] \cos f_0 - \right. \right. \\ & \left. \left. - e(-10 + 8\nu + e\nu \cos f_0) \cos 2f_0 \right) \right). \end{aligned} \quad (60)$$

In Equation (60), f_0 is the true anomaly at the initial epoch. In the test particle limit $\nu \rightarrow 0$, Equation (60) reduces to

$$\Delta T_{\text{ano}}^{1\text{pN}} = \frac{3\pi \sqrt{\mu a}}{c^2 (1-e^2)^2} \left[6 + 7e^2 + 2e^4 + 2e(7 + 3e^2) \cos f_0 + 5e^2 \cos 2f_0 \right]. \quad (61)$$

Figure 1 is obtained for generic values of the Keplerian orbital elements of a test particle revolving around a massive primary. It confirms the analytical result of Equation (61); over, say, three orbital revolutions, the satellite reaches always the precessing line of apsides after a time interval equal to $T_{\text{ano}}^{1\text{pN}}$. It is longer than T_{K} , in agreement with Equation (61), which is always positive.

Furthermore, Figure 2 plots the final part of the time series of the cosine $\hat{\mathbf{r}} \cdot \hat{\mathbf{C}}$ of the angle between the position vector \mathbf{r} and the Laplace–Runge–Lenz unit vector $\hat{\mathbf{C}}$ versus time t , in units of T_{K} , for a numerically integrated fictitious test particle with and without Equation (14) starting in both cases from, say, the moving pericentre, i.e., for $\hat{\mathbf{r}}_0 \cdot \hat{\mathbf{C}}_0 = +1$. It can be seen that the orbiter comes back to the same position on the precessing line of apsides, i.e. it is $\hat{\mathbf{r}} \cdot \hat{\mathbf{C}} = +1$ again, just after $T_{\text{ano}}^{1\text{pN}} = T_{\text{K}} + \Delta T_{\text{ano}}^{1\text{pN}}$ differing from T_{K} by a (positive) amount, in agreement with Equation (61).

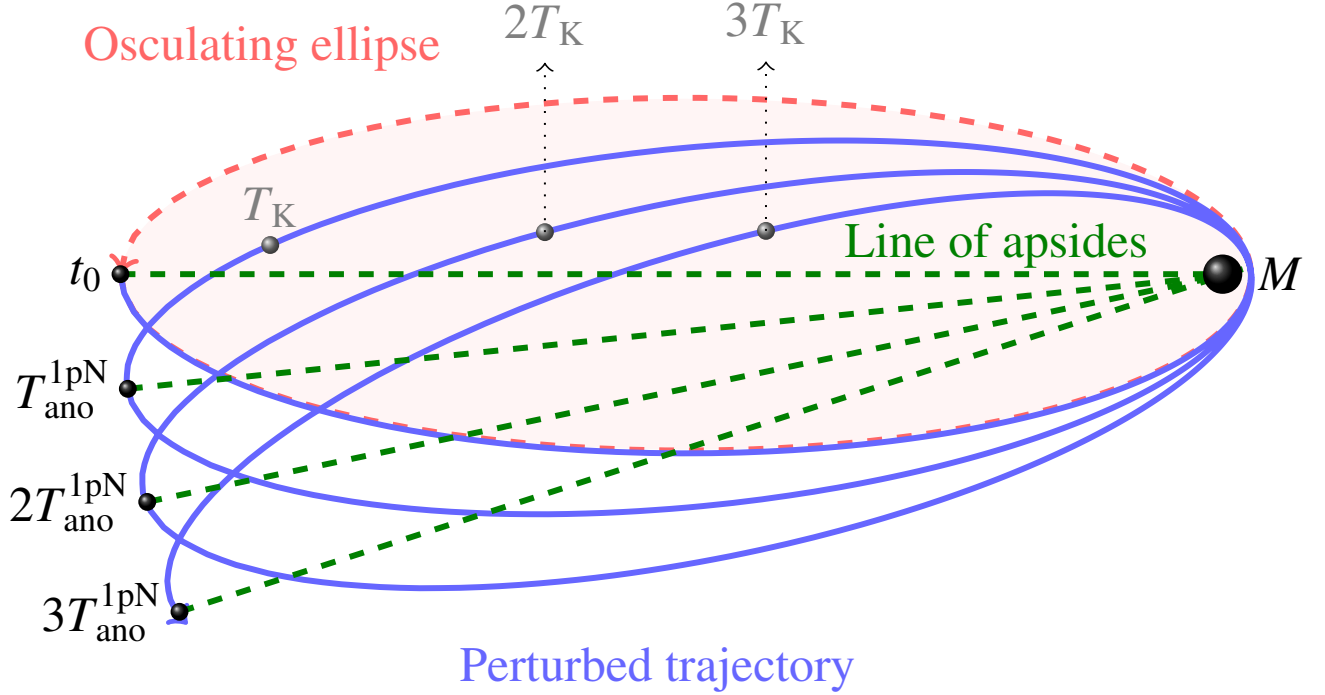


Figure 1. Perturbed 1pN trajectory (continuous blue curve) and its osculating Keplerian ellipse (dashed red curve) at the initial instant of time t_0 of a restricted two-body system characterized by $e = 0.95$, $I = 0$, $\Omega = 0$, $\omega = 90^\circ$, $f_0 = 180^\circ$ as seen from above the fixed orbital plane. Here, it is assumed that both ω and η undergo their known 1pN gravitoelectric secular precessions due to the mass M of the primary (Iorio 2017). For a better visualization of their effect, their sizes are suitably rescaled. The positions on the perturbed trajectory after one, two and three Keplerian periods T_K are marked in gray. At each orbit, the passages at the precessing dashed green line of apsides occur always later than in the Keplerian case by the amount given by Equation (61), which is always positive.

3.3. The 1pN gravitomagnetic Lense–Thirring correction

The LT anomalistic period can be calculated by means of Equations (30)–(32) as explained in Section 3.1. It turns out to be

$$T_{\text{ano}}^{\text{LT}} = T_K + \Delta T_{\text{ano}}^{\text{LT}}, \quad (62)$$

with

$$\Delta T_{\text{ano}}^{\text{LT}} = 0; \quad (63)$$

it is an exact result, valid to all orders in the eccentricity e .

Figure 3, obtained for generic values of the Keplerian orbital parameters, shows just that; over three orbital revolutions, the test particle reaches always the precessing line of apsides after a time interval equal to the Keplerian orbital period after each orbit.

Furthermore, Figure 4 plots the final part of the time series of the cosine $\hat{\mathbf{r}} \cdot \hat{\mathbf{C}}$ of the angle between the position vector \mathbf{r} and the Laplace–Runge–Lenz vector \mathbf{C} versus time t , in units of T_K , for a numerically integrated fictitious test particle acted upon by Equation (22) starting from, say, the moving pericentre, i.e., for $\hat{\mathbf{r}}_0 \cdot \hat{\mathbf{C}}_0 = +1$. It can be seen that it comes back to the same position on the precessing line of apsides, i.e. it is $\hat{\mathbf{r}} \cdot \hat{\mathbf{C}} = +1$ again, just after one Keplerian orbital period.

The fact that the gravitomagnetic apsidal period is identical to the Keplerian one can be intuitively justified since there is no net shift per orbit of the mean anomaly at epoch η . Indeed, from Equation (58), one infers that η is proportional to t_p through n_K . Thus, since the latter stays constant because a is not secularly affected by the gravitomagnetic field, the rate of change of the mean anomaly at epoch is proportional to the opposite of the pace of variation of the time of passage at pericentre according to

$$\frac{d\eta}{dt} = -n_K \frac{dt_p}{dt}. \quad (64)$$

Should η increase, the crossing of the pericentre would be anticipated with respect to the Keplerian case since t_p would decrease, and vice versa. In this case, the variation of η would result in an orbit-by-orbit advance or delay of the passages at the pericentre, which does not occur in the present case because, in fact, $\langle d\eta/dt \rangle^{\text{LT}} = 0$.

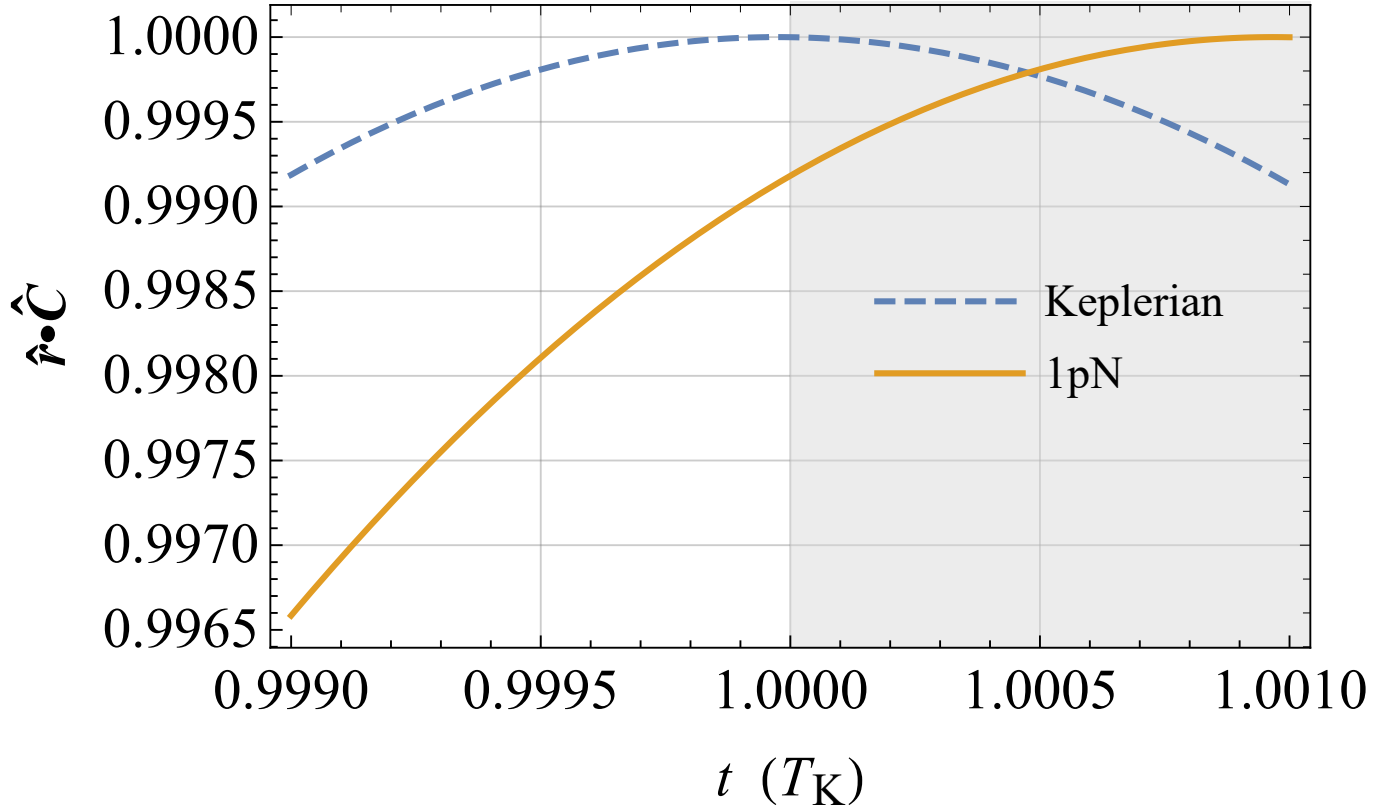


Figure 2. Numerically produced time series of the cosine $\hat{\mathbf{r}} \cdot \hat{\mathbf{C}}$ of the angle between the position vector \mathbf{r} and the Laplace–Runge–Lenz vector \mathbf{C} versus time t , in units of T_K , obtained by integrating the equations of motion of a fictitious test particle with (continuous ocre yellow curve) and without (dashed azure curve) the 1pN gravitoelectric acceleration of Equation (14) for an elliptical ($e = 0.665$) orbit arbitrarily oriented in space ($I = 40^\circ$, $\Omega = 45^\circ$, $\omega = 50^\circ$) starting from the periaxis ($f_0 = 0$), i.e., $\hat{\mathbf{r}}_0 \cdot \hat{\mathbf{C}}_0 = +1$; the semimajor axis is $a = 6R_e$. The physical parameters of the Earth are adopted. The 1pN acceleration is suitably rescaled in such a way that $\Delta T_{\text{ano}}^{1\text{pN}}/T_K = 0.001$. The time needed to come back to the initial position on the (moving) line of apsides, so that $\hat{\mathbf{r}} \cdot \hat{\mathbf{C}} = +1$ again, is longer than in the Keplerian case by the amount $\Delta T_{\text{ano}}^{1\text{pN}} = +0.001T_K$, shown by the shaded area, in agreement with Equation (61).

3.4. The Newtonian quadrupolar correction

The J_2 -affected anomalistic period can be calculated by means of Equations (41)–(43) as explained in Section 3.1. It turns out to be

$$T_{\text{ano}}^{J_2} = T_K + \Delta T_{\text{ano}}^{J_2}, \quad (65)$$

with

$$\Delta T_{\text{ano}}^{J_2} = \frac{3\pi J_2 R_e^2 (1 + e \cos f_0)^3}{2(1 - e^2)^3 \sqrt{\mu a}} \left(-2\widehat{T}_1 + 3\widehat{T}_2 + 3\widehat{T}_3 \cos 2u_0 + 6\widehat{T}_6 \sin 2u_0 \right). \quad (66)$$

Figure 5, obtained for generic values of the Keplerian orbital elements, confirms the analytical result of Equation (66); over three orbital revolutions, the test particle reaches always the precessing line of apsides after a time interval equal to $T_{\text{ano}}^{J_2}$ for each orbit. For the particular choice of the values of the primary's spin and orbital parameters, it turns out to be longer than T_K , in agreement with Equation (66).

Furthermore, Figure 6 plots the final part of the time series of the cosine $\hat{\mathbf{r}} \cdot \hat{\mathbf{C}}$ of the angle between the position vector \mathbf{r} and the Laplace–Runge–Lenz unit vector $\hat{\mathbf{C}}$ versus time t , in units of T_K , for a numerically integrated fictitious test particle with and without Equation (34) starting in both cases from, say, the moving pericentre, i.e., for $\hat{\mathbf{r}}_0 \cdot \hat{\mathbf{C}}_0 = +1$. It can be seen that it comes back to the same position on the precessing line of apsides, i.e. it is $\hat{\mathbf{r}} \cdot \hat{\mathbf{C}} = +1$ again, just after $T_{\text{ano}}^{J_2} = T_K + \Delta T_{\text{ano}}^{J_2}$ differing from T_K by a (positive) amount in agreement with Equation (66) for the particular choice of the generic values of the spin and the orbital parameters adopted in the numerical integrations.

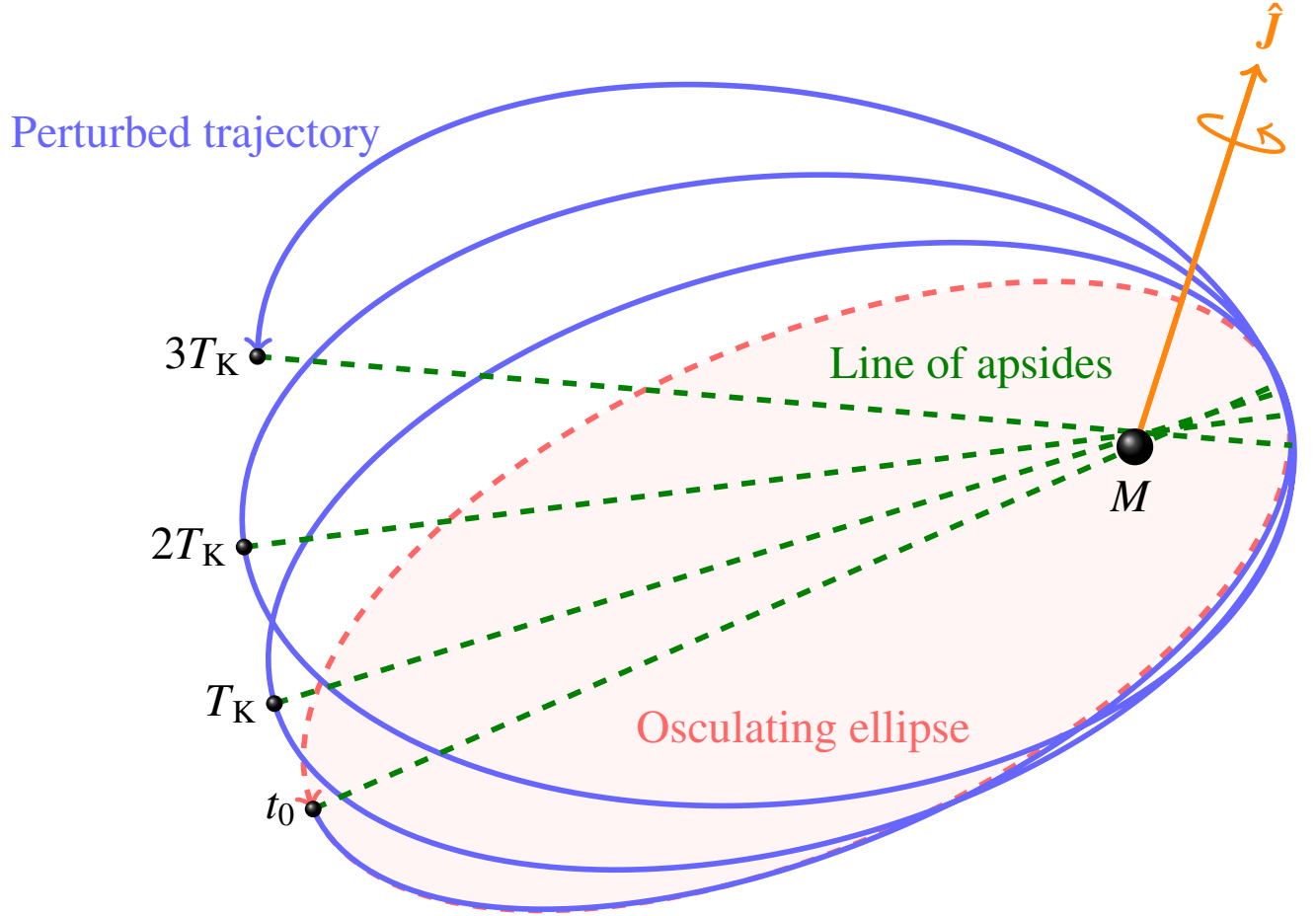


Figure 3. Perturbed LT trajectory (continuous blue curve) and its osculating Keplerian ellipse (dashed red curve) at the initial instant of time t_0 characterized by $e = 0.7$, $I = 30^\circ$, $\Omega = 72^\circ$, $\omega = 50^\circ$, $f_0 = 180^\circ$. The orientation of the spin axis \hat{J} of the central body is set by $\alpha_J = 45^\circ$, $\delta_J = 60^\circ$. In this example, I , Ω and ω undergo their known LT precessions due to the spin angular momentum \mathbf{J} of the primary (Iorio 2017); their magnitudes are suitably rescaled by enhancing them for a better visualisation. The initial position is chosen at the apocentre instead of the pericentre solely for the sake of better visualisation. The positions on the perturbed trajectory after one, two and three Keplerian periods are marked. At each orbit, the passage at the drifting dashed green line of apsides occurs always as in the Keplerian case because, according to Equation (63), $\Delta T_{\text{ano}}^{\text{LT}} = 0$.

4. The draconitic period

4.1. General calculational scheme

For a perturbed trajectory, the draconitic period T_{dra} is defined as the time interval between two successive instants when the real position of the test particle coincides with the ascending position on the corresponding osculating ellipse.

It can be calculated as (Mioc and Radu 1977; Iorio 2016)

$$T_{\text{dra}} = T_K + \Delta T_{\text{dra}} = \int_0^{2\pi} \left(\frac{dt}{du} \right) du, \quad (67)$$

where dt/du , when a pK perturbing acceleration A is present, can be obtained as follows.

From Equation (4) and Equation (48), one obtains (Ochocimski et al. 1959; Mioc and Radu 1977)

$$\frac{dt}{du} = \frac{\sqrt{\mu p}}{r^2} \left(1 - \frac{r^2 \cos I}{\sqrt{\mu p}} \frac{d\Omega}{dt} \right). \quad (68)$$

Then, it is

$$\frac{dt}{du} \simeq \frac{r^2}{\sqrt{\mu p}} + \frac{r^4 \cos I}{\mu p} \frac{d\Omega}{dt}. \quad (69)$$

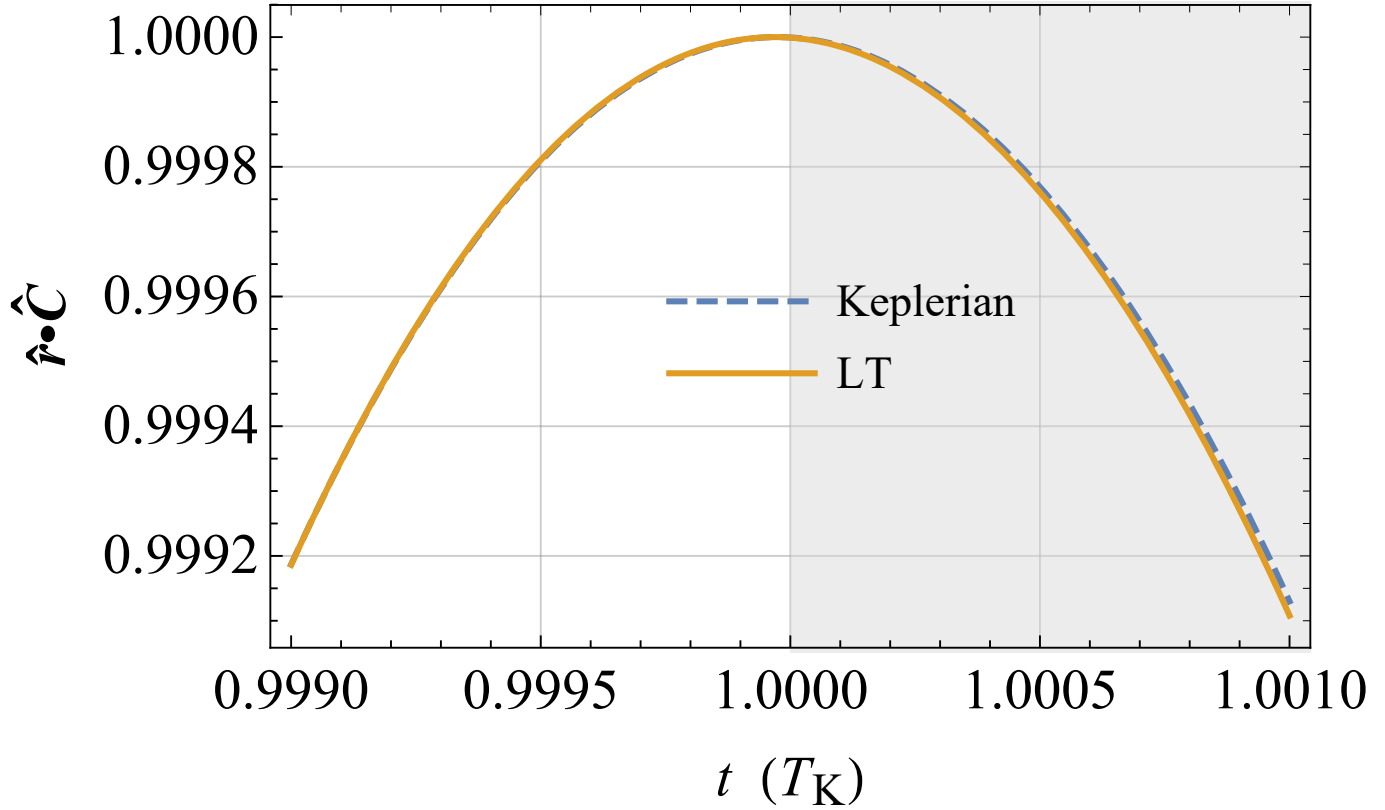


Figure 4. Numerically produced time series of the cosine $\hat{\mathbf{r}} \cdot \hat{\mathbf{C}}$ of the angle between the position vector \mathbf{r} and the Laplace–Runge–Lenz vector \mathbf{C} versus time t , in units of T_K , obtained by integrating the equations of motion of a fictitious test particle with (continuous orange yellow curve) and without (dashed azure curve) the LT acceleration of Equation (22) for an elliptical ($e = 0.665$) orbit arbitrarily oriented in space ($I = 40^\circ$, $\Omega = 45^\circ$, $\omega = 50^\circ$) starting from the periastron ($f_0 = 0$), i.e., $\hat{\mathbf{r}}_0 \cdot \hat{\mathbf{C}}_0 = +1$; the semimajor axis is $a = 6R_e$. The physical parameters of the Earth are adopted, apart from the spin axis position set by $\alpha_J = 45^\circ$, $\delta_J = 60^\circ$. The time needed to come back to the initial position on the (moving) line of apsides, so that $\hat{\mathbf{r}} \cdot \hat{\mathbf{C}} = +1$ again, is as in the Keplerian case.

Note that $d\Omega/dt$ is already expressed in terms of u , as per Equation (54). By using the nonsingular orbital elements⁸ (Mioc and Radu 1977; Montenbruck et al. 2006)

$$k := e \sin \omega, \quad (70)$$

$$q := e \cos \omega, \quad (71)$$

Equation (6) can be cast into the form

$$r = \frac{p}{1 + q \cos u + k \sin u} \quad (72)$$

in which p , q , k are treated as independent variables. By proceeding as in Section 3.1, it can be finally obtained (Mioc and Radu 1977; Iorio 2016)

$$\Delta T_{\text{dra}} = \int_0^{2\pi} \left\{ \frac{3}{2} \sqrt{\frac{p}{\mu}} \frac{\Delta p(u)}{(1 + q \cos u + k \sin u)^2} - 2 \sqrt{\frac{p^3}{\mu}} \frac{\cos u \Delta q(u) + \sin u \Delta k(u)}{(1 + q \cos u + k \sin u)^3} + \frac{r^4 \cos I}{\mu p} \frac{d\Omega}{dt} \right\} du. \quad (73)$$

⁸ They are the components of the eccentricity vector (Taff 1985), an alternative formulation of the Laplace–Runge–Lenz vector (Goldstein 1980). In the context of pulsar astronomy, they are also known as first and second Laplace–Lagrange parameters ϵ_1 , ϵ_2 (Lorimer and Kramer 2005).

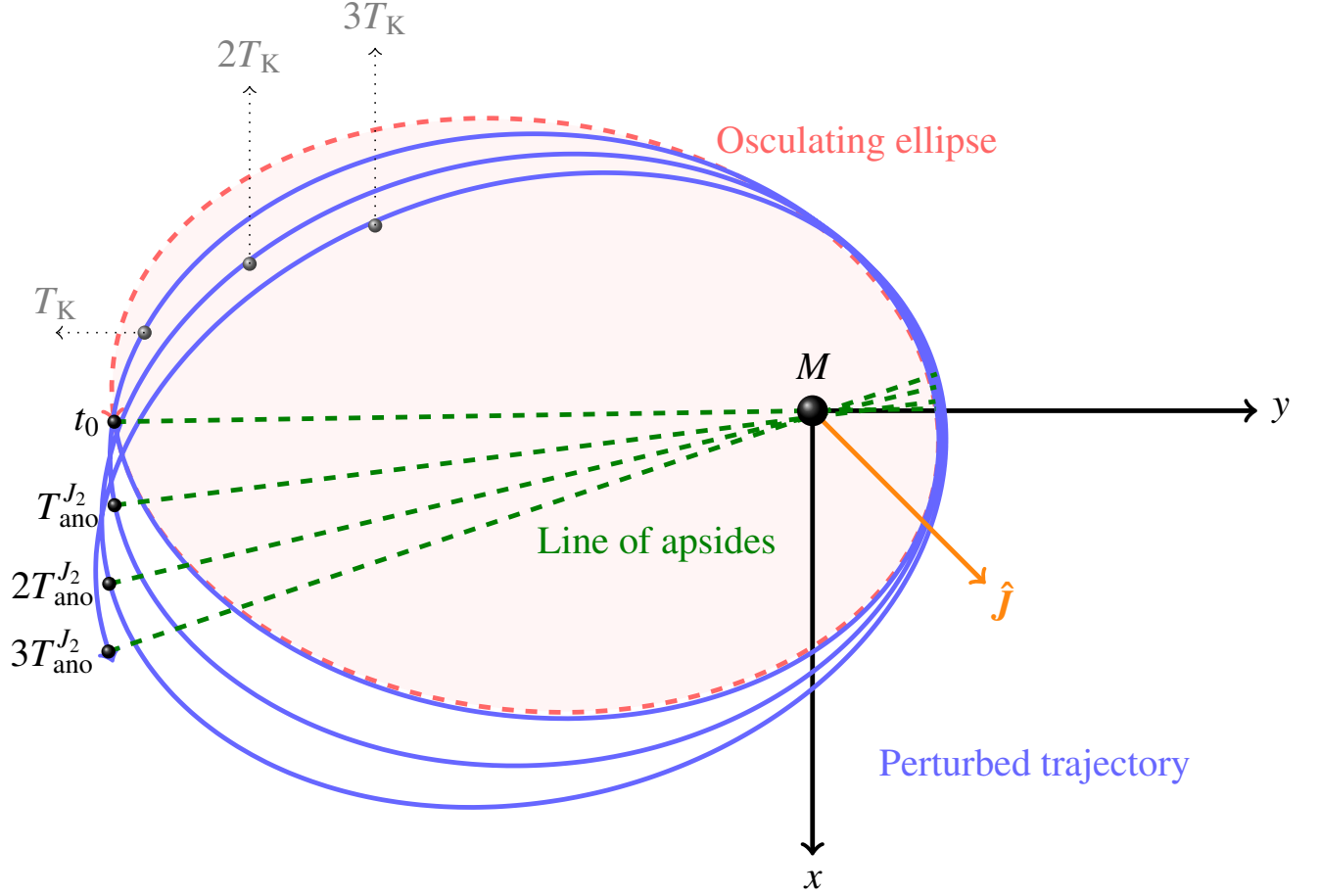


Figure 5. Perturbed J_2 trajectory (continuous blue curve) and its osculating Keplerian ellipse (dashed red curve) at the initial instant of time t_0 characterized by $e = 0.7$, $I = 30^\circ$, $\Omega = 45^\circ$, $\omega = 50^\circ$, $f_0 = 180^\circ$ as seen from the z -axis. The orientation of the spin axis $\hat{\mathbf{j}}$ of the central body is set by $\alpha_j = 45^\circ$, $\delta_j = 60^\circ$. In this example, I , Ω , ω and η undergo their known Newtonian precessions due to the quadrupole mass moment J_2 of the primary (Iorio 2017); their magnitudes are suitably rescaled by enhancing them for a better visualization. The positions on the perturbed trajectory after one, two and three Keplerian periods T_K are marked in gray. At each orbit, the passages at the drifting dashed green line of apsides occur always later than in the Keplerian case by the amount given by Equation (66), which is positive for the given values of the spin and orbital parameters.

The first-order variations $\Delta p(u)$, $\Delta q(u)$ and $\Delta k(u)$ entering Equation (73) are worked out by integrating the following expressions (Mioc and Radu 1977)

$$\frac{dp}{du} = \frac{2r^3 A_\tau}{\mu}, \quad (74)$$

$$\frac{dq}{du} = \frac{r^2 \sin u A_r}{\mu} + \frac{r^2 [r q + (r + p) \cos u] A_\tau}{\mu} + \frac{\cot I r^3 k \sin u A_h}{\mu p}, \quad (75)$$

$$\frac{dk}{du} = -\frac{r^2 \cos u A_r}{\mu} + \frac{r^2 [r k + (r + p) \sin u] A_\tau}{\mu} - \frac{\cot I r^3 q \sin u A_h}{\mu p} \quad (76)$$

from u_0 to u .

As far as the actual measurability of the draconitic period in some astronomical scenario of interest is concerned, it was shown (Amelin 1966; Kassimenko 1966; Zhongolovich 1966) that it is possible to measure it for an artificial Earth's satellite⁹ as the

⁹ In their analyses, Amelin (1966); Kassimenko (1966); Zhongolovich (1966) used the Soviet satellite 1960 ε 3.

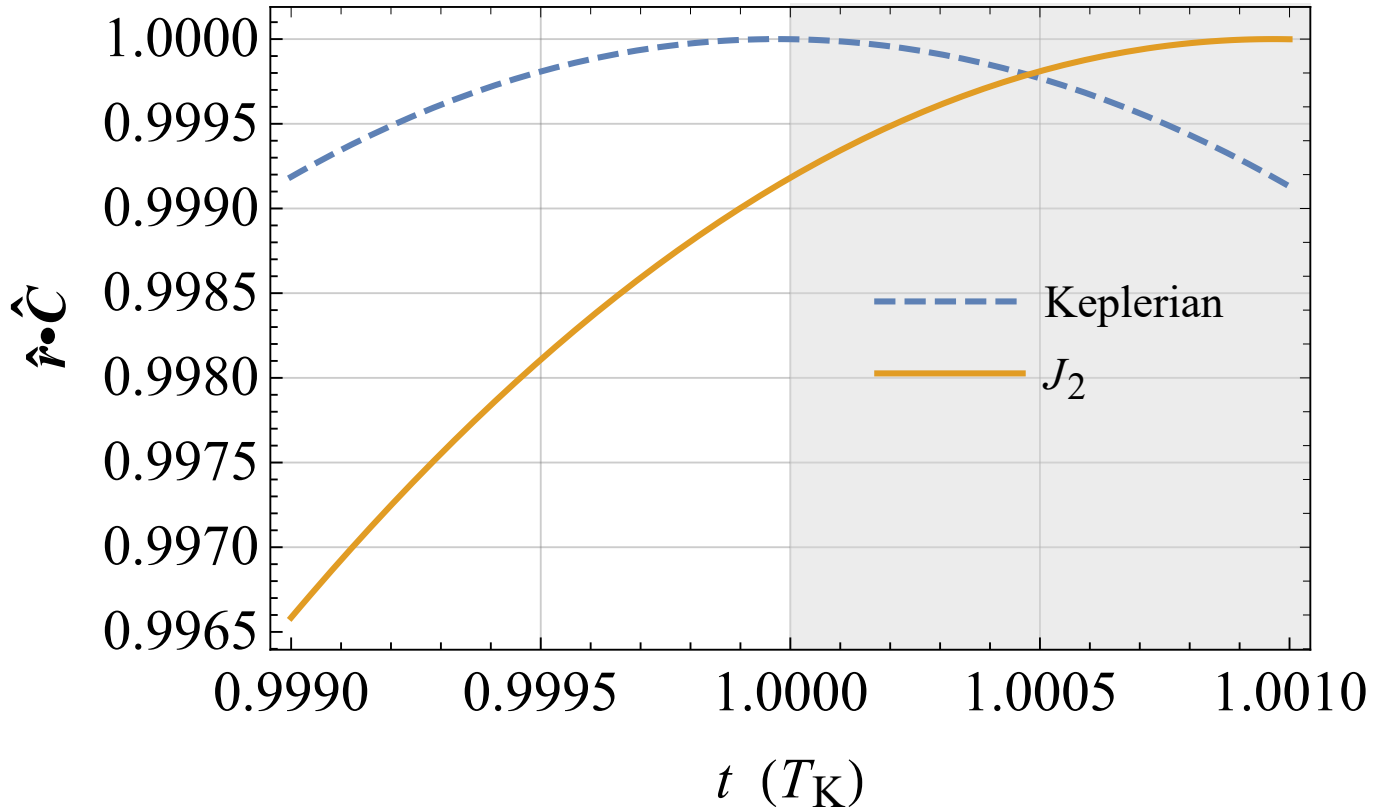


Figure 6. Numerically produced time series of the cosine $\hat{\mathbf{r}} \cdot \hat{\mathbf{C}}$ of the angle between the position vector \mathbf{r} and the Laplace–Runge–Lenz vector \mathbf{C} versus time t , in units of T_K , obtained by integrating the equations of motion of a fictitious test particle with (continuous ocrea yellow curve) and without (dashed azure curve) the J_2 acceleration of Equation (34) for an elliptical ($e = 0.665$) orbit arbitrarily oriented in space ($I = 40^\circ$, $\Omega = 45^\circ$, $\omega = 50^\circ$) starting from the periapsis ($f_0 = 0$), i.e., $\hat{\mathbf{r}}_0 \cdot \hat{\mathbf{C}}_0 = +1$; the semimajor axis is $a = 6R_e$. The physical parameters of the Earth are adopted, apart from the spin axis position set by $\alpha_J = 45^\circ$, $\delta_J = 60^\circ$. The J_2 acceleration is suitably rescaled in such a way that $|\Delta T_{\text{ano}}^{J_2}|/T_K = 0.001$. The time needed to come back to the initial position on the (moving) line of apsides, so that $\hat{\mathbf{r}} \cdot \hat{\mathbf{C}} = +1$ again, is longer than in the Keplerian case by the amount $\Delta T_{\text{ano}}^{J_2} = +0.001T_K$, shown by the shaded area, in agreement with Equation (66).

ratio of the difference of the times of passages of the sub-satellite point through a chosen parallel for two following epochs to the number of satellite revolutions corresponding to this difference. The accuracy reached at that time should be of the order of $\approx 10^{-4}$ s (Kassimenko 1966); it is not unlikely that it could be improved by orders of magnitude with the most recent techniques currently available.

4.2. The 1pN gravitoelectric correction

The 1pN draconitic period can be calculated by means of Equations (19)–(21) as explained in Section 4.1. It turns out to be

$$T_{\text{dra}}^{1\text{pN}} = T_K + \Delta T_{\text{dra}}^{1\text{pN}}, \quad (77)$$

with

$$\begin{aligned} \Delta T_{\text{dra}}^{1\text{pN}} = & \frac{\pi \sqrt{\mu_b a}}{4c^2} \left(72 + e^2 (84 - 76\nu) + 4e^4 (6 - 7\nu) - 16\nu - 3e \left[8(-7 + 3\nu) + e^2(-24 + 31\nu) \right] \cos f_0 + \right. \\ & \left. + e [4(-5 + 4\nu) \cos 2f_0 + e\nu \cos 3f_0] \right) - \frac{24 \sqrt{1 - e^2}}{(1 + e \cos \omega)^2}. \end{aligned} \quad (78)$$

In the test particle limit $\nu \rightarrow 0$, Equation (78) reduces to

$$\Delta T_{\text{dra}}^{1\text{pN}} = \frac{3\pi \sqrt{\mu a}}{c^2} \left[\frac{6 + 7e^2 + 2e^4 + 2e(7 + 3e^2) \cos f_0 + 5e^2 \cos 2f_0}{(1 - e^2)^2} - \frac{2 \sqrt{1 - e^2}}{(1 + e \cos \omega)^2} \right]. \quad (79)$$

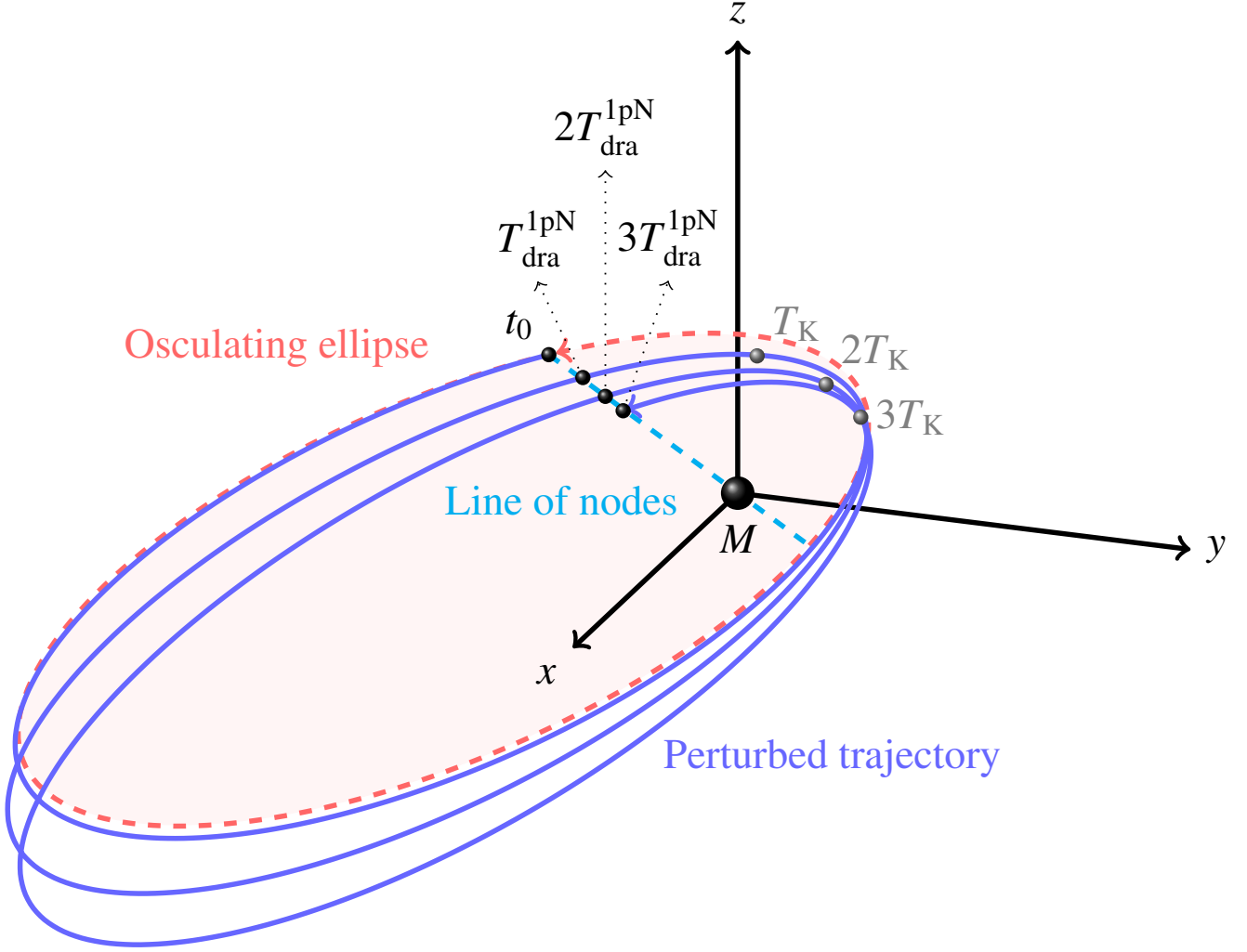


Figure 7. Perturbed 1pN trajectory (continuous blue curve) and its osculating Keplerian ellipse (dashed red curve) at the initial instant of time t_0 characterized by $e = 0.7$, $I = 30^\circ$, $\Omega = 45^\circ$, $\omega = 50^\circ$, $f_0 = 180^\circ - \omega$. In this example, it is assumed that both ω and η undergo the known 1pN gravitoelectric secular precessions due to the mass M of the primary (Iorio 2017). For a better visualization of their effect, their sizes are suitably rescaled. The positions on the perturbed trajectory after one, two and three Keplerian periods T_K are marked in gray. At each orbit, the passages at the fixed dashed cyan line of nodes occurs always later than in the Keplerian case by the amount given by Equation (79), which is always positive.

It can be noted that Equation (79) is always positive for all values of e , f_0 and ω ; thus, the node is reached later than in the Keplerian case.

Figure 7, obtained for generic values of the Keplerian orbital elements, confirms the analytical result of Equation (79); over, say, three orbital revolutions, the test particle reaches always the fixed line of nodes after a time interval equal to $T_{\text{dra}}^{1\text{pN}}$. It is longer than T_K , in agreement with Equation (79). Furthermore, Figure 8 plots the final part of the time series of the cosine $\hat{\mathbf{r}} \cdot \hat{\mathbf{l}}$ of the angle between the position vector \mathbf{r} and the node unit vector $\hat{\mathbf{l}}$ versus time t , in units of T_K , for a numerically integrated fictitious test particle with and without Equation (14) starting in both cases from, say, the fixed ascending node, i.e., for $\hat{\mathbf{r}}_0 \cdot \hat{\mathbf{l}}_0 = +1$. It can be seen that it comes back to the same position on the constant line of nodes, i.e. it is $\hat{\mathbf{r}} \cdot \hat{\mathbf{l}} = +1$ again, just after $T_{\text{dra}}^{1\text{pN}} = T_K + \Delta T_{\text{dra}}^{1\text{pN}}$ differing from T_K by a (positive) amount, in agreement with Equation (79).

4.3. The 1pN gravitomagnetic Lense–Thirring correction

The LT draconitic period can be calculated by means of Equations (30)–(32) as explained in Section 4.1. It turns out to be

$$T_{\text{dra}}^{\text{LT}} = T_K + \Delta T_{\text{dra}}^{\text{LT}}, \quad (80)$$

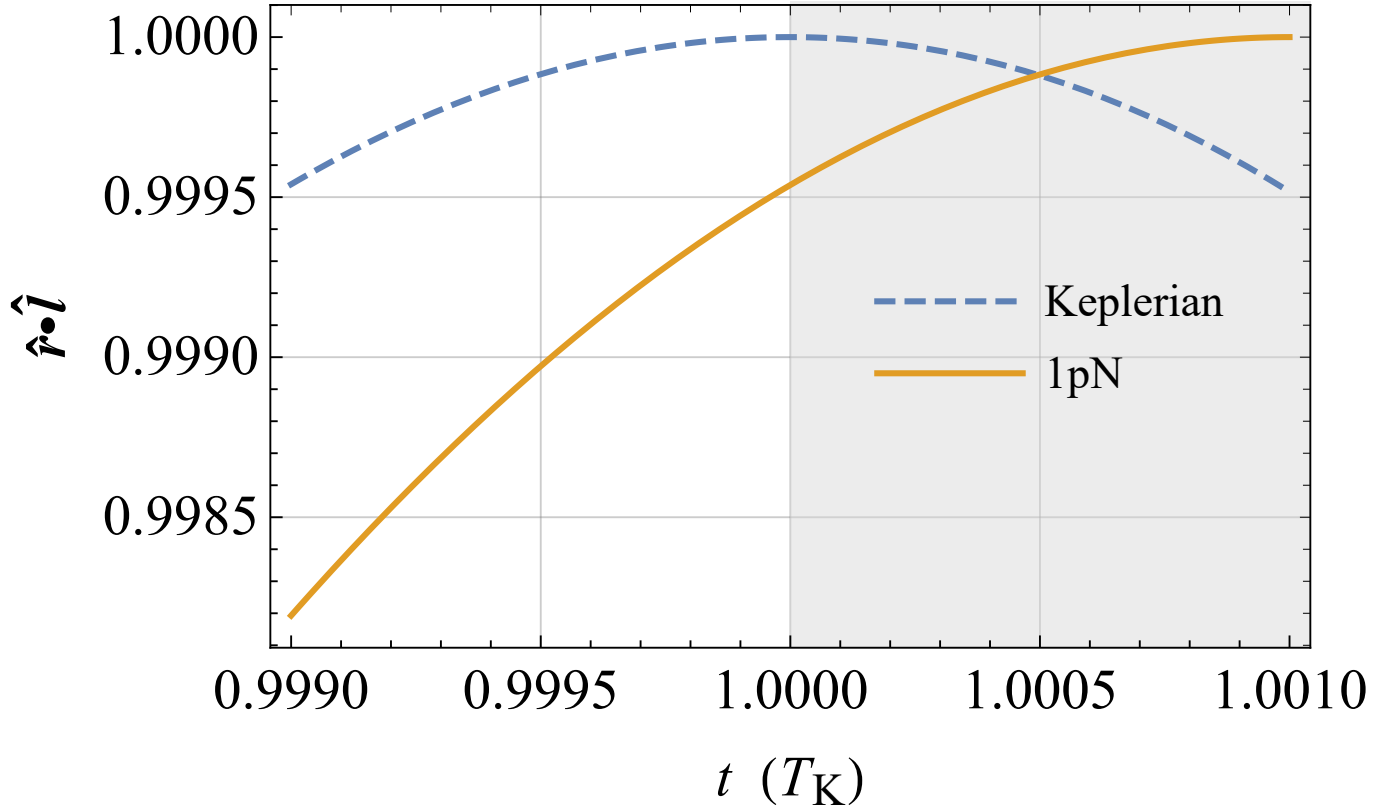


Figure 8. Numerically produced time series of the cosine $\hat{\mathbf{r}} \cdot \hat{\mathbf{l}}$ of the angle between the position vector \mathbf{r} and the node unit vector $\hat{\mathbf{l}}$ versus time t , in units of T_K , obtained by integrating the equations of motion of a fictitious test particle with (continuous orange curve) and without (dashed azure curve) the 1pN gravitoelectric acceleration of Equation (14) for an elliptical ($e = 0.665$) orbit arbitrarily oriented in space ($I = 40^\circ$, $\Omega = 45^\circ$, $\omega = 50^\circ$) starting from the ascending node \varnothing_Ω ($f_0 = -\omega + 360^\circ$), i.e., $\hat{\mathbf{r}}_0 \cdot \hat{\mathbf{l}}_0 = +1$; the semimajor axis is $a = 6R_e$. The physical parameters of the Earth are adopted. The 1pN acceleration is suitably rescaled in such a way that $\Delta T_{\text{dra}}^{\text{1pN}}/T_K = 0.001$. The time needed to come back to the initial position on the (fixed) line of nodes, so that $\hat{\mathbf{r}} \cdot \hat{\mathbf{l}} = +1$ again, is longer than in the Keplerian case by the amount $\Delta T_{\text{dra}}^{\text{1pN}} = +0.001T_K$, shown by the shaded area, in agreement with Equation (79).

with

$$\Delta T_{\text{dra}}^{\text{LT}} = \frac{4\pi J (2Jh + Jm \cot I)}{c^2 M (1 + e \cos \omega)^2}. \quad (81)$$

The explicit form of the geometric coefficient in the numerator of Equation (81) depending on the orientation in space of both the orbital plane and the primary's spin axis is

$$2Jh + Jm \cot I = 3 \cos I \sin \delta + \cos \delta (\csc I - 3 \sin I) \sin(\alpha_J - \Omega). \quad (82)$$

In general, it can be either positive and negative. For a polar orbit, i.e. for $\Omega = \alpha_J$ and $I = 90^\circ$, the gravitomagnetic correction vanishes, as per Equation (82). Instead, for an equatorial orbit arbitrarily oriented in space, it does not vanish amounting to

$$\Delta T_{\text{dra}}^{\text{LT}} = \pm \frac{8\pi J}{c^2 M (1 + e \cos \omega)^2}. \quad (83)$$

Furthermore, for circular orbits, Equation (83) reduces to

$$\Delta T_{\text{dra}}^{\text{LT}} = \pm \frac{8\pi J}{c^2 M}. \quad (84)$$

If the orbital plane lies in the reference plane, i.e. for $I = 0$, Equation (81) loses its meaning, as it is expected since, in this case, the line of nodes is no longer defined.

Figure 9, obtained for generic values of the Keplerian orbital parameters, confirms the analytical result of Equation (81); over three orbital revolutions, the test particle reaches always the precessing line of nodes after a time interval equal to $T_{\text{dra}}^{\text{LT}}$ after each

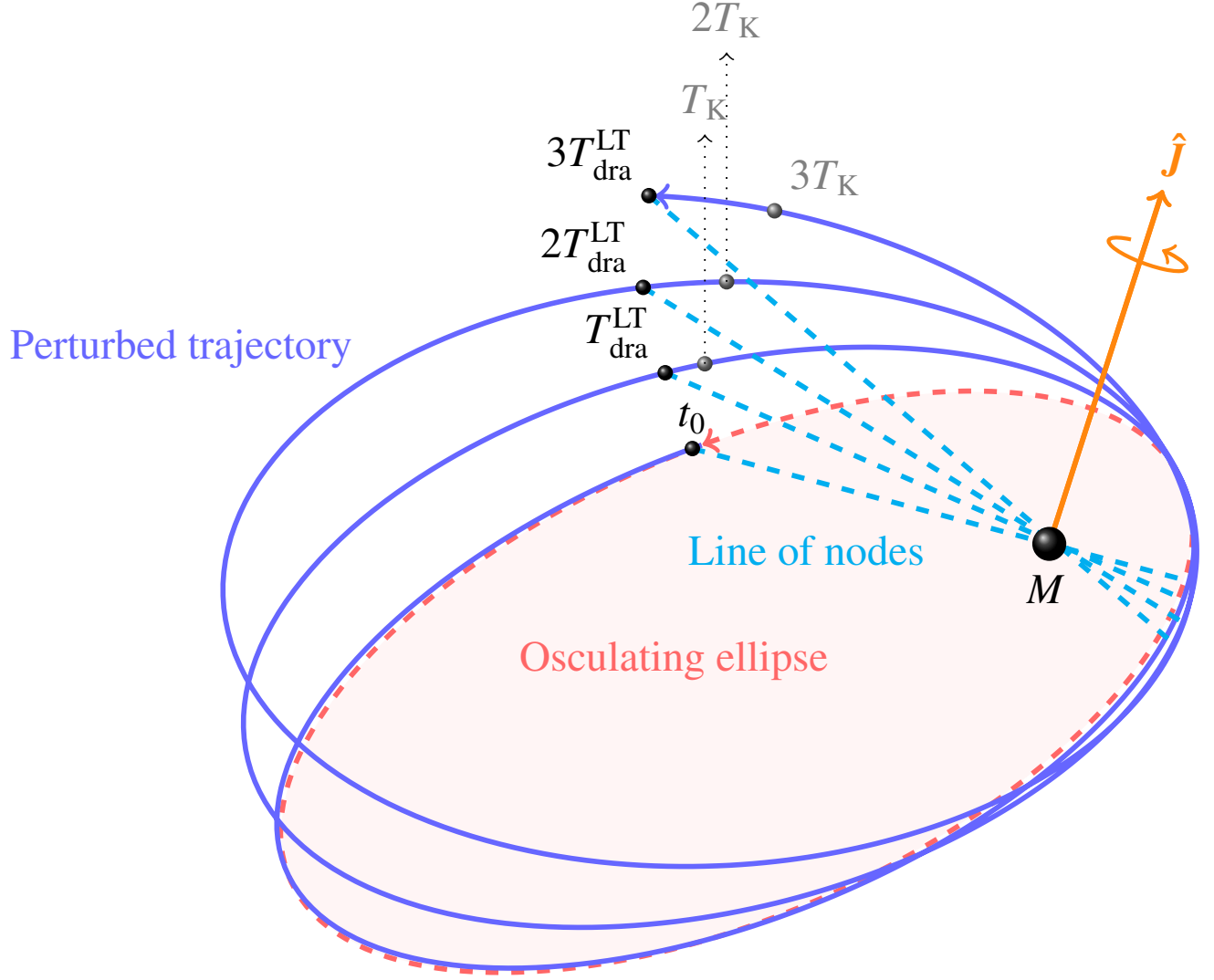


Figure 9. Perturbed LT trajectory (continuous blue curve) and its osculating Keplerian ellipse (dashed red curve) at the initial instant of time t_0 characterized by $e = 0.7$, $I = 30^\circ$, $\Omega = 72^\circ$, $\omega = 50^\circ$, $f_0 = 180^\circ - \omega$. The orientation of the spin axis $\hat{\mathbf{J}}$ of the central body is set by $\alpha_J = 45^\circ$, $\delta_J = 60^\circ$. In this example, I , Ω and ω undergo their known LT precessions due to the spin angular momentum \mathbf{J} of the primary (Iorio 2017); their magnitudes are suitably rescaled by enhancing them for a better visualisation. The positions on the perturbed trajectory after one, two and three Keplerian periods T_K are marked as well. At each orbit, the passages at the precessing dashed cyan line of nodes occur always later than in the Keplerian case by the amount given by Equation (81), which is positive for the given values of the spin and orbital parameters.

orbit. For the particular choice of the values of the primary and orbital parameters, it turns out to be longer than T_K , in agreement with Equation (81).

Furthermore, Figure 10 plots the final part of the time series of the cosine $\hat{\mathbf{r}} \cdot \hat{\mathbf{l}}$ of the angle between the position vector \mathbf{r} and the node unit vector $\hat{\mathbf{l}}$ versus time t , in units of T_K , for a numerically integrated fictitious test particle with and without Equation (22) starting in both cases from, say, the moving ascending node, i.e., for $\hat{\mathbf{r}}_0 \cdot \hat{\mathbf{l}}_0 = +1$. It can be seen that it comes back to the same position on the precessing line of nodes, i.e. it is $\hat{\mathbf{r}} \cdot \hat{\mathbf{l}} = +1$ again, just after $T_{\text{dra}}^{\text{LT}} = T_K + \Delta T_{\text{dra}}^{\text{LT}}$ differing from T_K by a (positive) amount, in agreement with Equation (81) for the particular choice of the generic values of the spin and the orbital parameters adopted in the numerical integrations.

4.4. The Newtonian quadrupolar correction

The J_2 -affected draconitic period can be calculated by means of Equations (41)–(43) as explained in Section 4.1. It turns out to be

$$T_{\text{dra}}^{J_2} = T_K + \Delta T_{\text{dra}}^{J_2}, \quad (85)$$

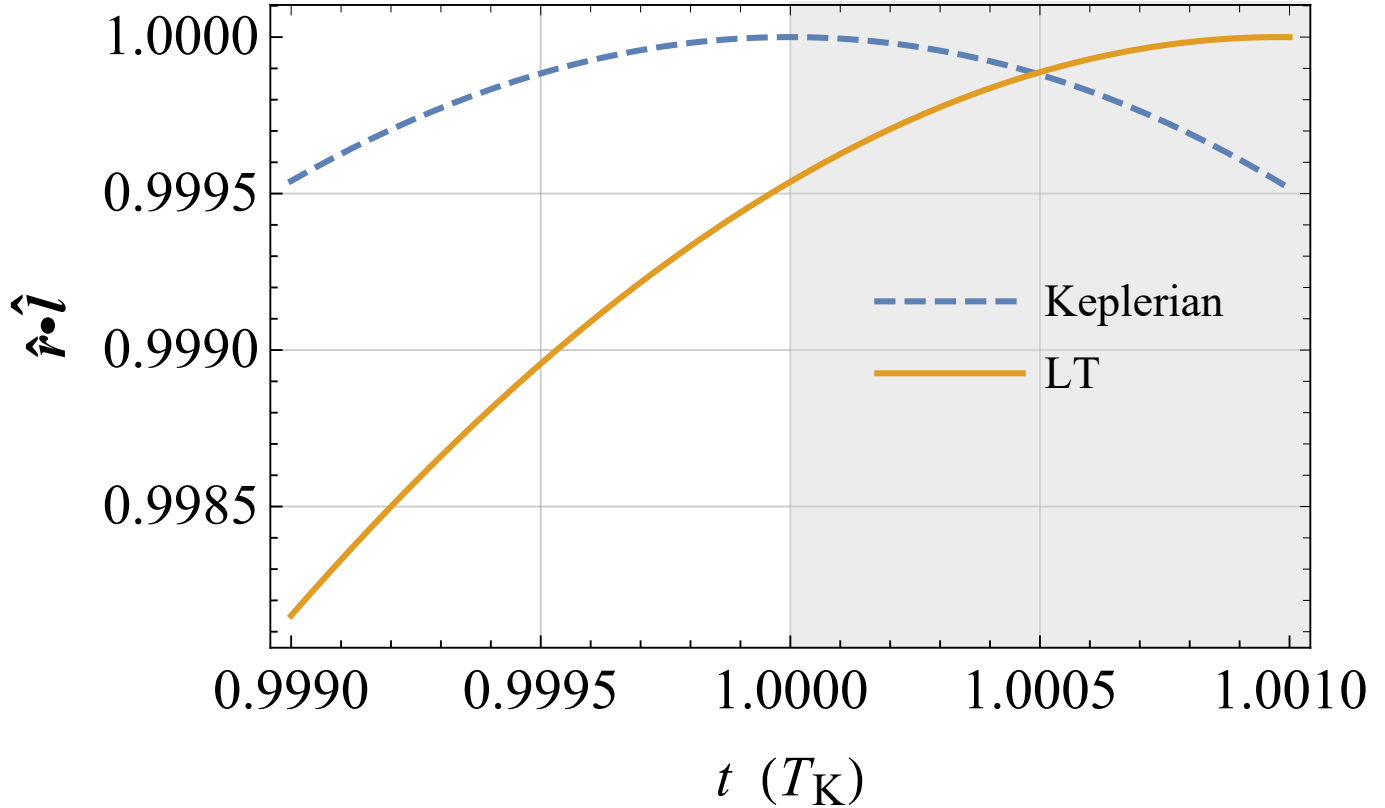


Figure 10. Numerically produced time series of the cosine $\hat{\mathbf{r}} \cdot \hat{\mathbf{l}}$ of the angle between the position vector \mathbf{r} and the node unit vector $\hat{\mathbf{l}}$ versus time t , in units of T_K , obtained by integrating the equations of motion of a fictitious test particle with (continuous orange yellow curve) and without (dashed azure curve) the LT acceleration of Equation (22) for an elliptical ($e = 0.665$) orbit arbitrarily oriented in space ($I = 40^\circ$, $\Omega = 45^\circ$, $\omega = 50^\circ$) starting from the ascending node \varOmega ($f_0 = -\omega + 360^\circ$), i.e., $\hat{\mathbf{r}}_0 \cdot \hat{\mathbf{l}}_0 = +1$; the semimajor axis is $a = 6R_e$. The physical parameters of the Earth are adopted, apart from the spin axis position set by $\alpha_J = 45^\circ$, $\delta_J = 60^\circ$. The LT acceleration is suitably rescaled in such a way that $|\Delta T_{\text{dra}}^{\text{LT}}|/T_K = 0.001$. The time needed to come back to the initial position on the (moving) line of nodes, so that $\hat{\mathbf{r}} \cdot \hat{\mathbf{l}} = +1$ again, is longer than in the Keplerian case by the amount $\Delta T_{\text{dra}}^{\text{LT}} = +0.001T_K$, shown by the shaded area, in agreement with Equation (81).

with

$$\Delta T_{\text{dra}}^{J_2} = \frac{3\pi J_2 R_e^2}{2\sqrt{\mu a(1-e^2)}} \left[\frac{1}{(1+e\cos\omega)^2} (-2\widehat{T}_1 + 3\widehat{T}_2 - 2\widehat{T}_5 \cot I) + \frac{(1+e\cos f_0)^3}{(1-e^2)^{5/2}} (-2\widehat{T}_1 + 3\widehat{T}_2 + 3\widehat{T}_3 \cos 2u_0 + 6\widehat{T}_6 \sin 2u_0) \right]. \quad (86)$$

It can be noted that Equation (86) is not defined for $I \rightarrow 0$ because of the term

$$\widehat{T}_5 \cot I = \cot I [\sin I \sin \delta_J + \cos I \cos \delta_J \sin(\alpha_J - \Omega)] [\cos I \sin \delta_J - \cos \delta_J \sin I \sin(\alpha_J - \Omega)],$$

as it is expected since, in this case, the line of nodes is no longer defined.

Figure 11, obtained for generic values of the Keplerian orbital elements, confirms the analytical result of Equation (86); over three orbital revolutions, the test particle reaches always the precessing line of nodes after a time interval equal to $T_{\text{dra}}^{J_2}$ after each orbit. For the particular choice of the values of the primary's spin and orbital parameters, it is shorter than T_K , in agreement with Equation (86).

Furthermore, Figure 12 plots the final part of the time series of the cosine $\hat{\mathbf{r}} \cdot \hat{\mathbf{l}}$ of the angle between the position vector \mathbf{r} and the node unit vector $\hat{\mathbf{l}}$ versus time t , in units of T_K , for a numerically integrated fictitious test particle with and without Equation (34) starting in both cases from, say, the moving ascending node, i.e., for $\hat{\mathbf{r}}_0 \cdot \hat{\mathbf{l}}_0 = +1$. It can be seen that it comes back to the same position on the precessing line of nodes, i.e. it is $\hat{\mathbf{r}} \cdot \hat{\mathbf{l}} = +1$ again, just after $T_{\text{dra}}^{J_2} = T_K + \Delta T_{\text{dra}}^{J_2}$ differing from T_K by a (positive) amount in agreement with Equation (86) for the particular choice of the generic values of the spin and the orbital parameters adopted in the numerical integrations.

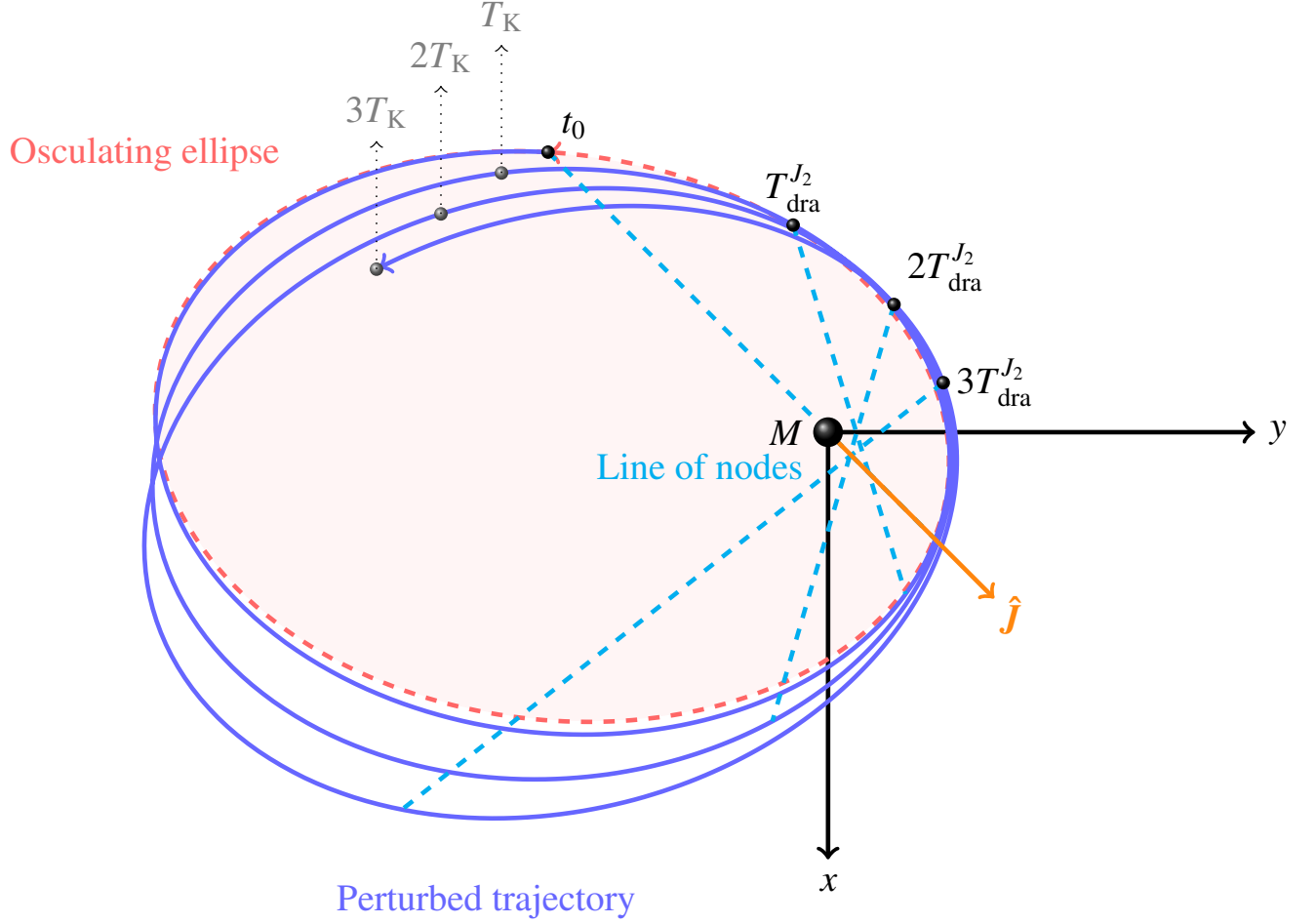


Figure 11. Perturbed J_2 trajectory (continuous blue curve) and its osculating Keplerian ellipse (dashed red curve) at the initial instant of time t_0 characterized by $e = 0.7$, $I = 30^\circ$, $\Omega = 45^\circ$, $\omega = 50^\circ$, $f_0 = 180^\circ - \omega$ as seen from the z -axis. The orientation of the spin axis $\hat{\mathbf{j}}$ of the central body is set by $\alpha_J = 45^\circ$, $\delta_J = 60^\circ$. In this example, I , Ω , ω and η undergo their known Newtonian shifts due to the quadrupole mass moment J_2 of the primary (Iorio 2017); their magnitudes are suitably rescaled for better visualizing their effect. The positions on the perturbed trajectory after one, two and three Keplerian periods T_K are marked in gray. At each orbit, the passages at the precessing dashed cyan line of nodes occur always earlier than in the Keplerian case by the amount given by Equation (86), which is negative for the given values of the spin and orbital parameters.

5. The sidereal period

5.1. General calculational scheme

In general, both the line of nodes and the line of apsides do vary over time because of one or more pK accelerations. Thus, it may be useful to look at a characteristic orbital timescale involving the crossing of some fixed reference direction in space; the sidereal period T_{sid} , defined as the time interval between two successive instants when the real position of the test particle lies on a given reference direction, plays well such a role.

For an orbit arbitrarily inclined, the sidereal period can be calculated as

$$T_{\text{sid}} = T_K + \Delta T_{\text{sid}} = \int_0^{2\pi} \left(\frac{dt}{d\phi} \right) d\phi, \quad (87)$$

where $\phi(t)$ is the azimuthal angle reckoned from the reference x axis in the fundamental plane; when the latter is assumed to be coincident with, say, the Earth's equatorial plane at some reference epoch, $\phi(t)$ is the right ascension $\alpha(t)$ of the celestial body of

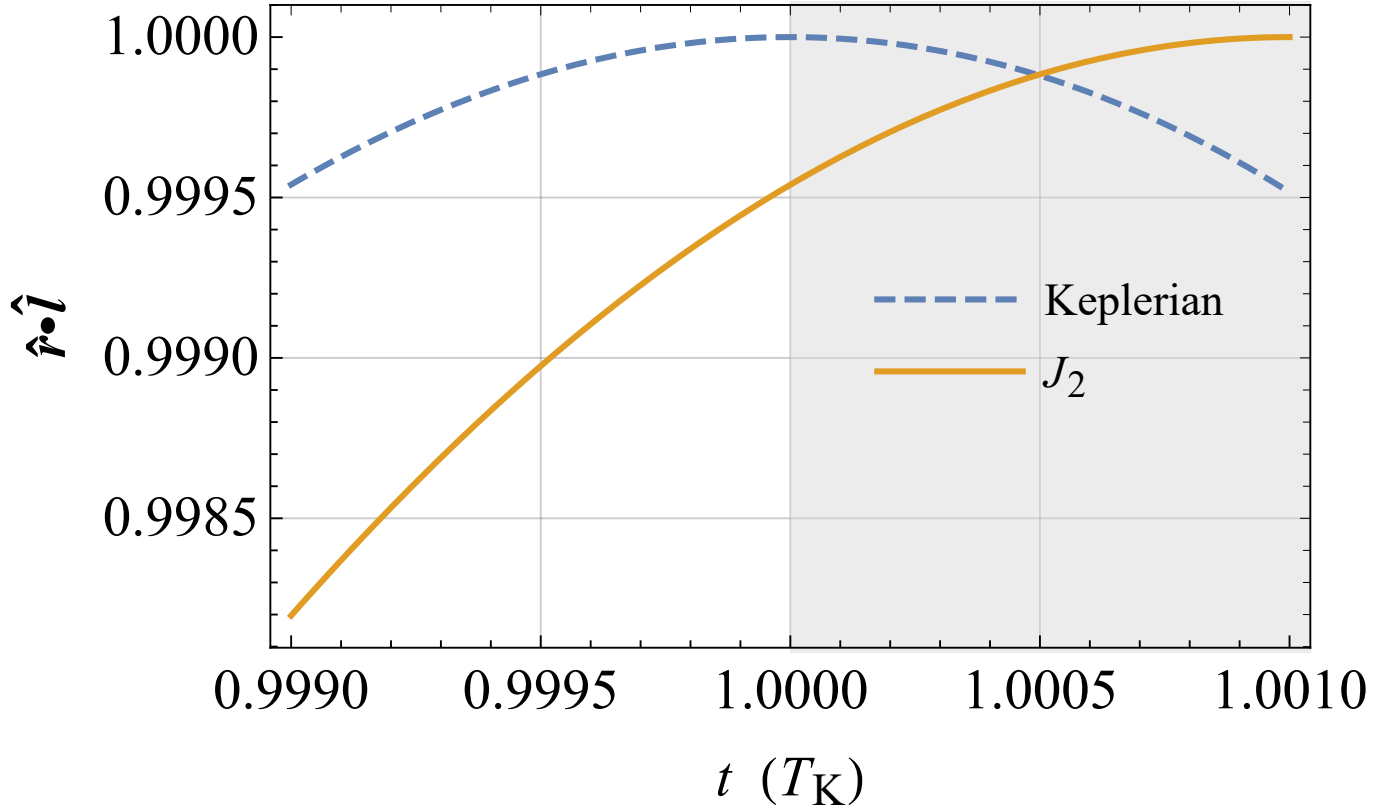


Figure 12. Numerically produced time series of the cosine $\hat{\mathbf{r}} \cdot \hat{\mathbf{l}}$ of the angle between the position vector \mathbf{r} and the node unit vector $\hat{\mathbf{l}}$ versus time t , in units of T_K , obtained by integrating the equations of motion of a fictitious test particle with (continuous ocra yellow curve) and without (dashed azure curve) the J_2 acceleration of Equation (34) for an elliptical ($e = 0.665$) orbit arbitrarily oriented in space ($I = 40^\circ$, $\Omega = 45^\circ$, $\omega = 50^\circ$) starting from the ascending node \varOmega ($f_0 = -\omega + 360^\circ$), i.e., $\hat{\mathbf{r}}_0 \cdot \hat{\mathbf{l}}_0 = +1$; the semimajor axis is $a = 6R_e$. The physical parameters of the Earth are adopted, apart from the spin axis position set by $\alpha_J = 45^\circ$, $\delta_J = 60^\circ$. The J_2 acceleration is suitably rescaled in such a way that $|\Delta T_{\text{dra}}^{J_2}|/T_K = 0.001$. The time needed to come back to the initial position on the (moving) line of nodes, so that $\hat{\mathbf{r}} \cdot \hat{\mathbf{l}} = +1$ again, is longer than in the Keplerian case by the amount $\Delta T_{\text{dra}}^{J_2} = +0.001T_K$, shown by the shaded area, in agreement with Equation (86).

interest. From

$$x(t) = r(t) [\cos \Omega \cos u(t) - \cos I \sin \Omega \sin u(t)], \quad (88)$$

$$y(t) = r(t) [\sin \Omega \cos u(t) + \cos I \cos \Omega \sin u(t)], \quad (89)$$

one obtains $\phi(t)$ as

$$\phi(t) = \arctan \left[\frac{y(t)}{x(t)} \right]; \quad (90)$$

it is a function of the generally varying $I(t)$, $\Omega(t)$, and of $u(t)$, i.e. $\phi(t) = \phi(I(t), \Omega(t), u(t))$. Since the ongoing calculation is to the first order in the pK acceleration, the differential $d\phi$ in Equation (87) can be written as

$$d\phi \simeq \left(\frac{\partial \phi}{\partial u} \right) du. \quad (91)$$

The integrand of Equation (87) can be obtained as

$$\frac{dt}{d\phi} = \frac{1}{\frac{d\phi}{dt}} = \frac{1}{\frac{\partial \phi}{\partial I} \frac{dI}{dt} + \frac{\partial \phi}{\partial \Omega} \frac{d\Omega}{dt} + \frac{\partial \phi}{\partial u} \frac{du}{dt}} = \frac{1}{\frac{du}{dt} \frac{\partial \phi}{\partial u} \left[1 + \frac{\partial u}{\partial \phi} \left(\frac{\partial \phi}{\partial I} \frac{dI}{dt} + \frac{\partial \phi}{\partial \Omega} \frac{d\Omega}{dt} \right) \right]}. \quad (92)$$

Thus, to the first order in the pK acceleration, the integral of Equation (87) can be approximated as

$$T_{\text{sid}} \simeq \int_0^{2\pi} \frac{dt}{du} \left[1 - \frac{\partial u}{\partial \phi} \left(\frac{\partial \phi}{\partial I} \frac{dI}{du} + \frac{\partial \phi}{\partial \Omega} \frac{d\Omega}{du} \right) \right] du = \int_0^{2\pi} \left(\frac{dt}{du} \right) du - \int_0^{2\pi} \frac{1}{\frac{\partial \phi}{\partial u}} \left(\frac{\partial \phi}{\partial I} \frac{dI}{du} + \frac{\partial \phi}{\partial \Omega} \frac{d\Omega}{du} \right) \left(\frac{dt}{du} \right) du. \quad (93)$$

The first term in Equation (93) is nothing but the draconitic period, and can be calculated to the order $O(A)$ as outlined in Section 4.1. The second term in Equation (93) is a correction to the former

$$\Delta T_{\text{sid II}} := - \int_0^{2\pi} \frac{1}{\frac{\partial \phi}{\partial u}} \left(\frac{\partial \phi}{\partial I} \frac{dI}{du} + \frac{\partial \phi}{\partial \Omega} \frac{d\Omega}{du} \right) \left(\frac{dt}{du} \right)_K du. \quad (94)$$

taking into account the fact that, in general, the orbital plane is displaced by the pK acceleration; indeed, the rates of I and Ω enter it. In Equation (94), the suffix K appended to dt/du implies that it has to be calculated onto the unperturbed Keplerian ellipse in order to keep the calculation to the first order in A .

If the orbital plane coincides with the fundamental one, the previously outlined calculational strategy may lead to analytical expressions for T_{sid} which, for some pK accelerations, are singular in $I = 0$. In that cases, the sidereal period can be straightforwardly calculated by means of the true longitude

$$l := \varpi + f, \quad (95)$$

where

$$\varpi := \Omega + \omega \quad (96)$$

is the longitude of pericentre¹⁰, as (Iorio 2016)

$$T_{\text{sid}} = T_K + \Delta T_{\text{sid}} = \int_0^{2\pi} \left(\frac{dt}{dl} \right) dl, \quad (97)$$

in close analogy with Section 3.1 and Section 4.1. It should be recalled that l is generally a dogleg angle since Ω and u are located in different planes; it is the true longitude of the test particle actually moving along its real orbit only if $I = 0$. When a pK perturbing acceleration A enters the equations of motion, dt/dl can be obtained in the following way.

From Equation (111) and Equation (47), it is

$$\frac{dl}{dt} = \frac{\sqrt{\mu p}}{r^2} \left[1 + \frac{2r^2 \sin^2(I/2)}{\sqrt{\mu p}} \frac{d\Omega}{dt} \right]. \quad (98)$$

Then, it can be written

$$\frac{dt}{dl} \simeq \frac{r^2}{\sqrt{\mu p}} - \frac{2r^4 \sin^2(I/2)}{\mu p} \frac{d\Omega}{dt}. \quad (99)$$

The sine of the argument of latitude u entering Equation (54) for $d\Omega/dt$ can be written in terms of l as $\sin(l - \Omega)$. By introducing the nonsingular equinoctial elements (Broucke and Cefola 1972)

$$Q := e \cos \varpi, \quad (100)$$

$$K := e \sin \varpi, \quad (101)$$

Equation (6) can be rewritten as

$$r = \frac{p}{1 + Q \cos l + K \sin l} \quad (102)$$

in which p , Q , K are to be treated as independent variables. By proceeding as in Section 3.1 and Section 4.1, one obtains (Iorio 2016)

$$\Delta T_{\text{sid}} = \int_0^{2\pi} \left\{ \frac{3}{2} \sqrt{\frac{p}{\mu}} \frac{\Delta p(l)}{(1 + Q \cos l + K \sin l)^2} - 2 \sqrt{\frac{p^3}{\mu}} \frac{\cos l \Delta Q(l) + \sin l \Delta K(l)}{(1 + Q \cos l + K \sin l)^3} - \frac{2r^4 \sin^2(I/2)}{\mu p} \frac{d\Omega}{dt} \right\}_K dl. \quad (103)$$

¹⁰ It is a dogleg angle (Murray and Dermott 1999; Shevchenko 2017) since Ω and ω lie generally in different planes.

The first-order variations $\Delta p(l)$, $\Delta Q(l)$ and $\Delta K(l)$ entering Equation (103) can be worked out by integrating the following expressions (Iorio 2016)

$$\frac{dp}{dl} = \frac{2r^3 A_\tau}{\mu}, \quad (104)$$

$$\frac{dQ}{dl} = \frac{r^2 \sin l A_r}{\mu} + \frac{r^2 [r Q + (r+p) \cos l] A_\tau}{\mu} - \frac{\tan(I/2) r^3 K \sin(l-\Omega) A_h}{\mu p}, \quad (105)$$

$$\frac{dK}{dl} = -\frac{r^2 \cos l A_r}{\mu} + \frac{r^2 [r K + (r+p) \sin l] A_\tau}{\mu} + \frac{\tan(I/2) r^3 Q \sin(l-\Omega) A_h}{\mu p} \quad (106)$$

from l_0 to l . If the orbital plane is aligned with the fundamental one, Equation (103) and Equations (105)–(106) have to be calculated with $I = 0$.

It is generally expected that if the orbital plane stays constant in space, i.e. if neither the nodes, when defined, nor the orbit's projection onto the fundamental plane change over time, the sidereal period coincides with the draconitic one since the line of nodes is a fixed direction in space.

5.2. The $1pN$ gravitoelectric correction

As shown in Section 5.1, the sidereal period for a generic perturbed orbit is the sum of the draconitic period, calculated as explained in Section 4.1, and the term given by Equation (94). For Equation (14), Equation (94) turns out to be

$$\Delta T_{\text{sid II}}^{1pN} = 0. \quad (107)$$

Thus, in this case, the sidereal period coincides with the draconitic one.

This is shown in Figure 13. It plots the final part of the time series of the cosine of the angle ϕ , normalized to its initial value $\cos \phi_0$, versus time t , in units of T_K , for a numerically integrated fictitious test particle with and without Equation (14) starting from the same generic initial position. It can be seen that it comes back to the same position on the fixed direction chosen in the reference plane, i.e. it is $\cos \phi / \cos \phi_0 = +1$ again, just after $T_{\text{sid}}^{1pN} = T_{\text{dra}}^{1pN}$ differing from T_K by a positive amount, in agreement with Equation (79).

5.3. The $1pN$ gravitomagnetic Lense–Thirring correction

As shown in Section 5.1, the sidereal period for a generic perturbed orbit is the sum of the draconitic period, calculated as explained in Section 4.1, and the term given by Equation (94). For Equation (22), Equation (94) yields

$$\Delta T_{\text{sid II}}^{\text{LT}} = \frac{4\pi J \cot I}{c^2 M e^2 \sqrt{1-e^2}} \cdot \left\{ \hat{\mathbf{m}} \left[-e^2 + 2(2-e^2-2\sqrt{1-e^2}) \cos 2\omega \right] + 2\hat{\mathbf{l}} \left(-2 + e^2 + 2\sqrt{1-e^2} \right) \sin 2\omega \right\}. \quad (108)$$

In the equatorial case, the orbital plane stays constant in space, Equation (108) vanishes, and the sidereal period coincides with the draconitic one, as it is expected since neither the line of nodes nor the orbit's projection onto the reference plane change. By taking the sum of Equation (81) and Equation (108), the full expression of the gravitomagnetic correction of the sidereal period $\Delta T_{\text{sid}}^{\text{LT}}$ is obtained. It can be noted that, for a generic eccentric orbit, $\Delta T_{\text{sid}}^{\text{LT}}$ is not defined if the orbital plane lies in the fundamental one. Nonetheless, for $e = 0$, it reduces to

$$\Delta T_{\text{sid}}^{\text{LT}} = \frac{8\pi J}{c^2 M} [\cos I \sin \delta_J - \cos \delta_J \sin I \sin(\alpha_J - \Omega)], \quad (109)$$

which is not singular in $I = 0$. By using the true longitude l in the case $I = 0$, it turns out

$$\Delta T_{\text{sid}}^{\text{LT}} = \frac{8\pi J \sin \delta_J}{c^2 M (1 + e \cos \varpi)^2}. \quad (110)$$

In the limit $e \rightarrow 0$, it reduces to

$$\Delta T_{\text{sid}}^{\text{LT}} = \frac{8\pi J \sin \delta_J}{c^2 M}, \quad (111)$$

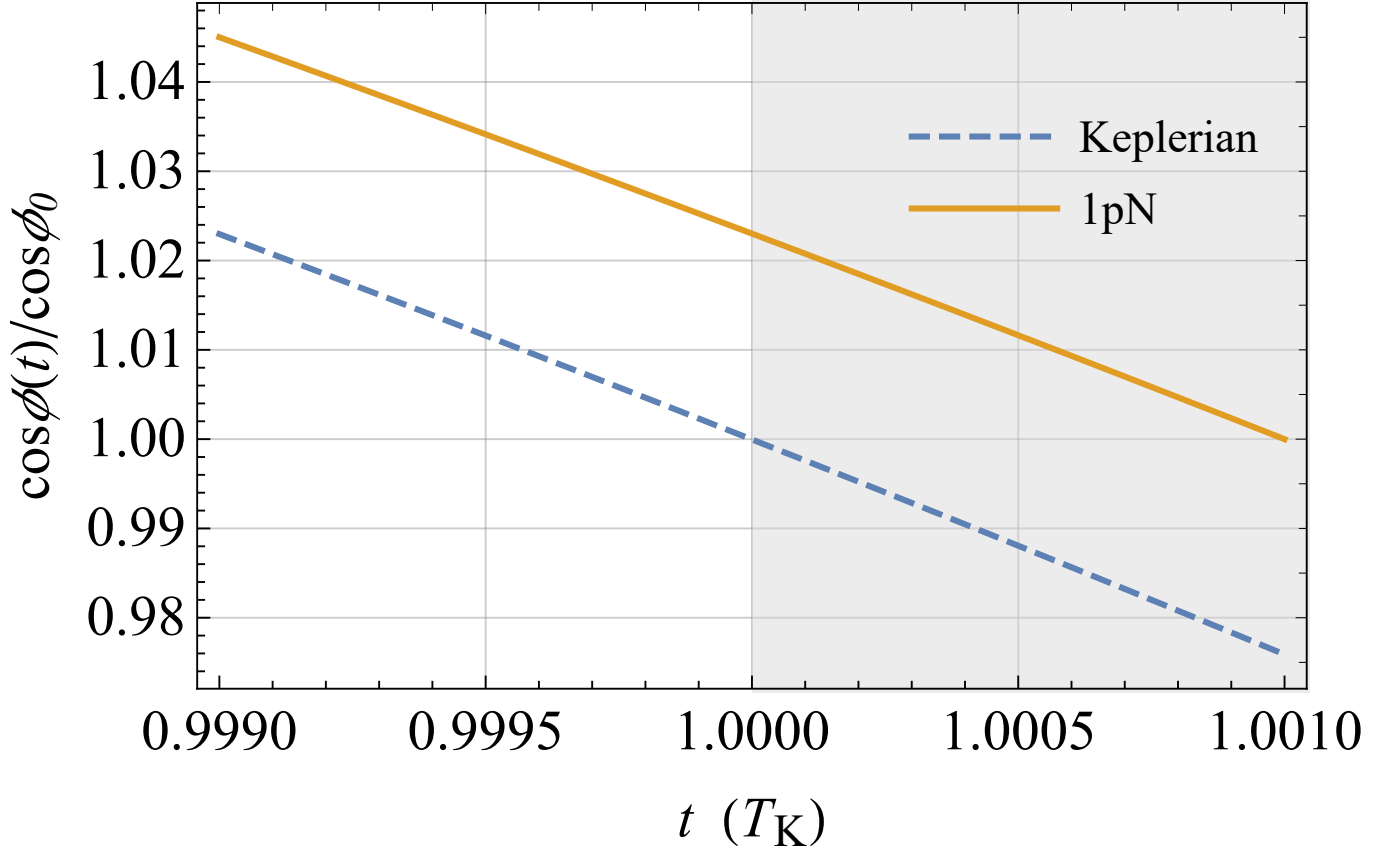


Figure 13. Numerically produced time series of the cosine $\cos \phi(t)$ of the azimuthal angle $\phi(t)$ normalized to its initial value $\cos \phi_0$ versus time t , in units of T_K , obtained by integrating the equations of motion of a fictitious test particle with (continuous orange curve) and without (dashed azure curve) the 1pN gravitoelectric acceleration of Equation (14) for an elliptical ($e = 0.665$) orbit arbitrarily oriented in space ($I = 40^\circ$, $\Omega = 45^\circ$, $\omega = 50^\circ$) starting from, say, the ascending node δ_ζ ($f_0 = -\omega + 360^\circ$); the semimajor axis is $a = 6R_e$. The physical parameters of the Earth are adopted. The 1pN acceleration is suitably rescaled in such a way that $\Delta T_{\text{sid}}^{\text{1pN}}/T_K = 0.001$. The time needed to $\cos \phi(t)$ to assume again its initial value $\cos \phi_0$ is longer than in the Keplerian case by the amount $\Delta T_{\text{sid}}^{\text{1pN}} = +0.001T_K$, shown by the shaded area, in agreement with the sum of Equation (79).

which agrees with Equation (109) calculated with $I = 0$. In turn, if $\delta_J = \pm 90^\circ$, corresponding to the case of an equatorial orbit whose orbital plane coincides with the reference plane, Equation (111) becomes

$$\Delta T_{\text{sid}}^{\text{LT}} = \pm \frac{8\pi J}{c^2 M}, \quad (112)$$

in agreement with Equation (84).

Figure 14 confirms the analytical results of Equation (81) and Equation (108). Indeed, over three orbital revolutions, the projection of a generic LT perturbed orbit in the fundamental plane $\{x, y\}$ crosses a fixed direction in the latter set by a certain value ϕ_0 always after a time interval equal to $T_{\text{sid}}^{\text{LT}} = T_{\text{dra}}^{\text{LT}} + \Delta T_{\text{sid II}}^{\text{LT}}$ for each orbit. With the particular choice of the primary's spin and the orbital parameters used in the picture, $T_{\text{sid}}^{\text{LT}}$ turns out to be shorter than T_K , in agreement with Equation (81) and Equation (108).

Furthermore, Figure 15 plots the final part of the time series of the cosine of the angle ϕ , normalized to its initial value $\cos \phi_0$, versus time t , in units of T_K , for a numerically integrated fictitious test particle with and without Equation (22) starting from the same generic initial position. It can be seen that it comes back to the same position on the fixed direction chosen in the reference plane, i.e. it is $\cos \phi / \cos \phi_0 = +1$ again, just after $T_{\text{sid}}^{\text{LT}} = T_{\text{dra}}^{\text{LT}} + \Delta T_{\text{sid II}}^{\text{LT}}$ differing from T_K by a (positive) amount in agreement with Equation (81) and Equation (108) for the particular choice of the generic values of the spin and the orbital parameters adopted in the numerical integrations.

5.4. The Newtonian quadrupolar correction

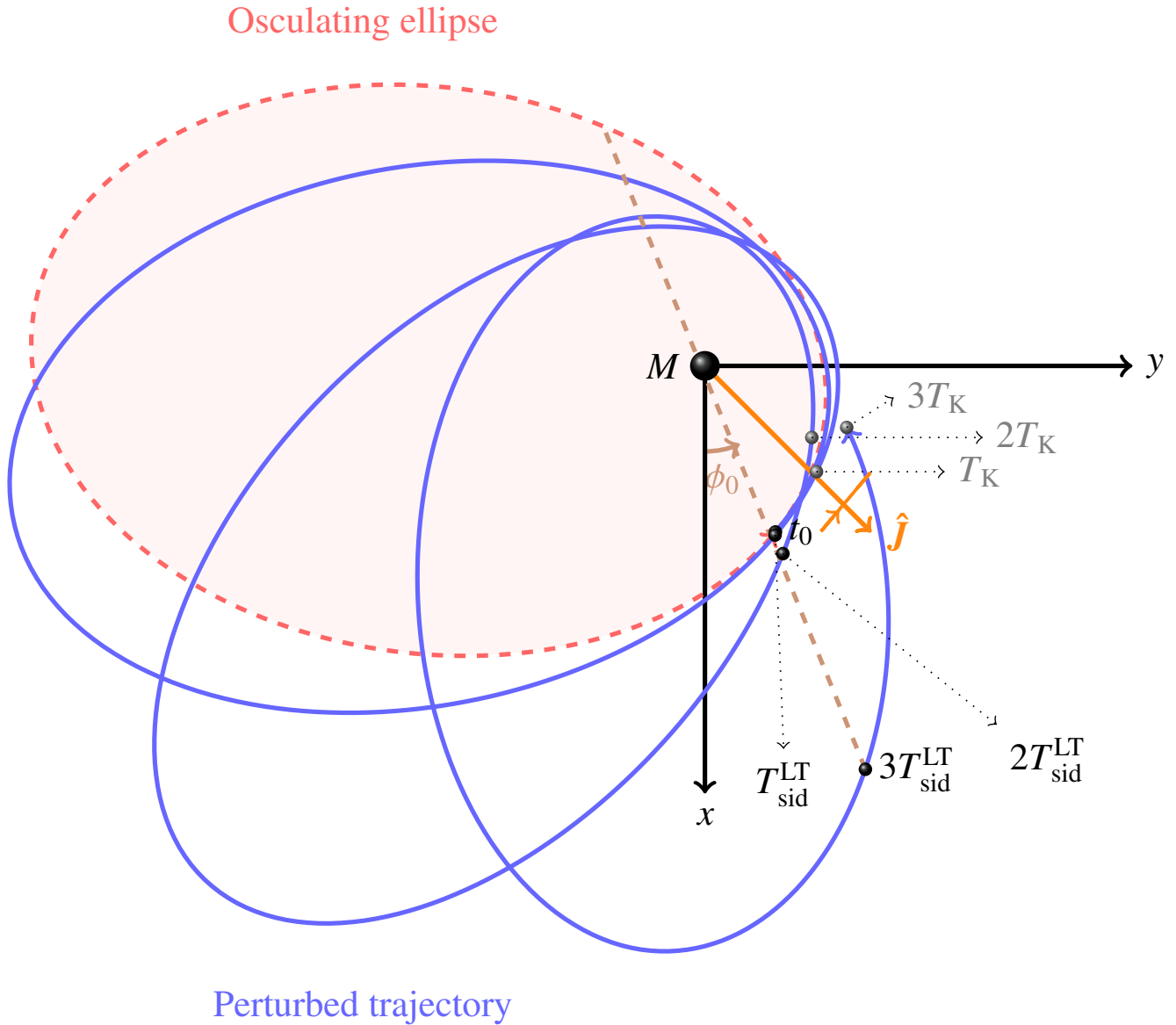


Figure 14. Projections of the perturbed LT trajectory (continuous blue curve) and of its osculating Keplerian ellipse (dashed red curve) in the reference plane $\{x, y\}$ at the initial instant of time t_0 characterized by the generic initial conditions $e = 0.7$, $I = 30^\circ$, $\Omega = 45^\circ$, $\omega = 50^\circ$, $f_0 = 285^\circ$. The orientation of the spin axis $\hat{\mathbf{J}}$ of the central body, whose projection in the fundamental plane is depicted as well, is set by $\alpha_J = 45^\circ$, $\delta_J = 60^\circ$. In this example, I , Ω , and ω undergo their known LT shifts due to the spin angular momentum \mathbf{J} of the primary (Iorio 2017); their sizes are suitably rescaled for better visualizing their effect. The positions on the perturbed trajectory after one, two and three Keplerian periods T_K are marked as well. At each orbit, the passages at the generic fixed dashed brown line characterized by ϕ_0 occur always earlier than in the Keplerian case by the amount given by the sum of Equation (81) and Equation (108). It is so because, for the given values of the spin and orbital parameters, $\Delta T_{\text{dra}}^{\text{LT}} + \Delta T_{\text{sid II}}^{\text{LT}} < 0$, as per Equation (81) and Equation (108).

As shown in Section 5.1, the sidereal period for a generic perturbed orbit is the sum of the draconitic period, calculated as explained in Section 4.1, and the term given by Equation (94). For Equation (34), Equation (94) turns out to be

$$\Delta T_{\text{sid II}}^{J_2} = \frac{3\pi J_2 R_c^2 \cot I}{e^2 \sqrt{\mu a (1 - e^2)}} \left\{ \widehat{T}_5 \left[e^2 + 2(-2 + e^2 + 2\sqrt{1 - e^2}) \cos 2\omega \right] - 2\widehat{T}_4 \left(-2 + e^2 + 2\sqrt{1 - e^2} \right) \sin 2\omega \right\}. \quad (113)$$

For equatorial orbits, Equation (113) vanishes, and the sidereal period reduces to the draconitic one. The oblateness of the sidereal period $\Delta T_{\text{sid}}^{J_2}$ can be obtained by summing Equation (86) and Equation (113); for an elliptic orbit, it turns out to be singular in

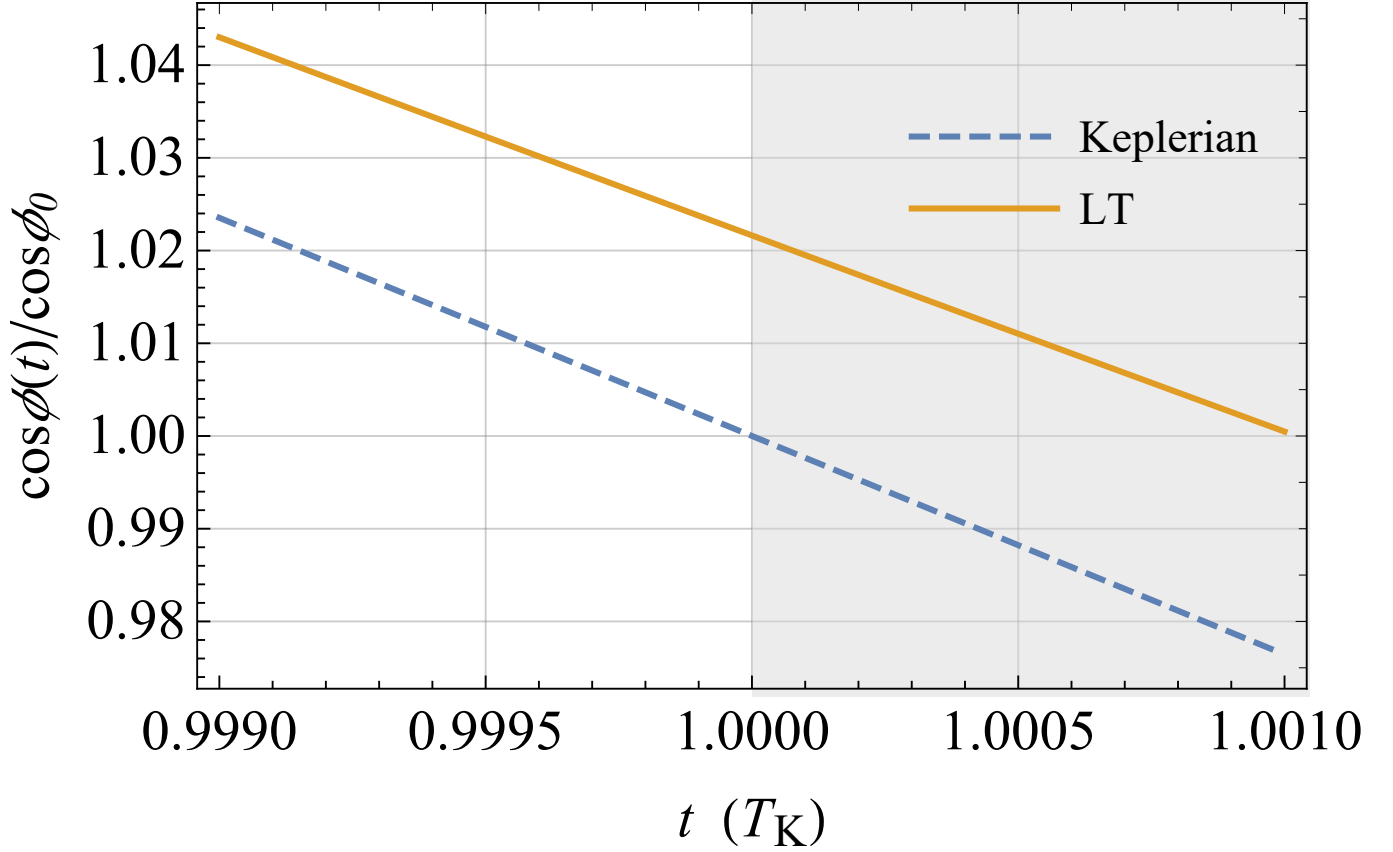


Figure 15. Numerically produced time series of the cosine $\cos \phi(t)$ of the azimuthal angle $\phi(t)$ normalized to its initial value $\cos \phi_0$ versus time t , in units of T_K , obtained by integrating the equations of motion of a fictitious test particle with (continuous ocre yellow curve) and without (dashed azure curve) the LT acceleration of Equation (22) for an elliptical ($e = 0.665$) orbit arbitrarily oriented in space ($I = 40^\circ$, $\Omega = 45^\circ$, $\omega = 310^\circ$) starting from, say, $f_0 = 50^\circ$; the semimajor axis is $a = 6R_e$. The physical parameters of the Earth are adopted, apart from the spin axis position set by $\alpha_J = 45^\circ$, $\delta_J = 60^\circ$. The LT acceleration is suitably rescaled in such a way that $|\Delta T_{\text{sid}}^{\text{LT}}|/T_K = 0.001$. The time needed to $\cos \phi(t)$ to assume again its initial value $\cos \phi_0$ is longer than in the Keplerian case by the amount $\Delta T_{\text{sid}}^{\text{LT}} = +0.001T_K$, shown by the shaded area, in agreement with the sum of Equation (81) and Equation (108).

$I = 0$. Instead, in the limit $e \rightarrow 0$, it reduces to

$$\begin{aligned} \Delta T_{\text{sid}}^{J_2} = & \frac{3\pi J_2 R_e^2}{2\sqrt{\mu a}} \left\{ -4 + 6 \cos^2 \delta_J \cos^2 (\alpha_J - \Omega) + 6 \cos \delta_J \cos (\alpha_J - \Omega) \sin 2u_0 [\sin I \sin \delta_J + \cos I \cos \delta_J \sin (\alpha_J - \Omega)] + \right. \\ & + 6 [\sin I \sin \delta_J + \cos I \cos \delta_J \sin (\alpha_J - \Omega)]^2 + 3 \cos 2u_0 [\cos \delta_J \cos (\alpha_J - \Omega) - \sin I \sin \delta_J - \cos I \cos \delta_J \sin (\alpha_J - \Omega)] \times \\ & \left. \times [\cos \delta_J \cos (\alpha_J - \Omega) + \sin I \sin \delta_J + \cos I \cos \delta_J \sin (\alpha_J - \Omega)] \right\}, \end{aligned} \quad (114)$$

which is defined also for that value of the inclination. In such a case, using the true longitude l yields

$$\begin{aligned} \Delta T_{\text{sid}}^{J_2} = & -\frac{3\pi J_2 R_e^2}{4(1-e^2)^2 \sqrt{\mu a}} \left[\frac{(-2 + 3 \cos^2 \delta_J)}{(1 + e \cos \varpi)^2} \left[2 + e^2 - 2(1 - e^2)^{3/2} + 4e \cos \varpi + e^2 \cos 2\varpi \right] + \right. \\ & \left. + \frac{1}{2(1 - e^2)} \left((4 + e^2)(1 - 3 \cos 2\delta_J) - e \left[-1 + 6 \cos^2 (l_0 - \alpha_J) \cos 2\delta_J \right] [3e \cos (2l_0 - 2\varpi) + 6 \cos (l_0 - \varpi) + \right. \right. \end{aligned}$$

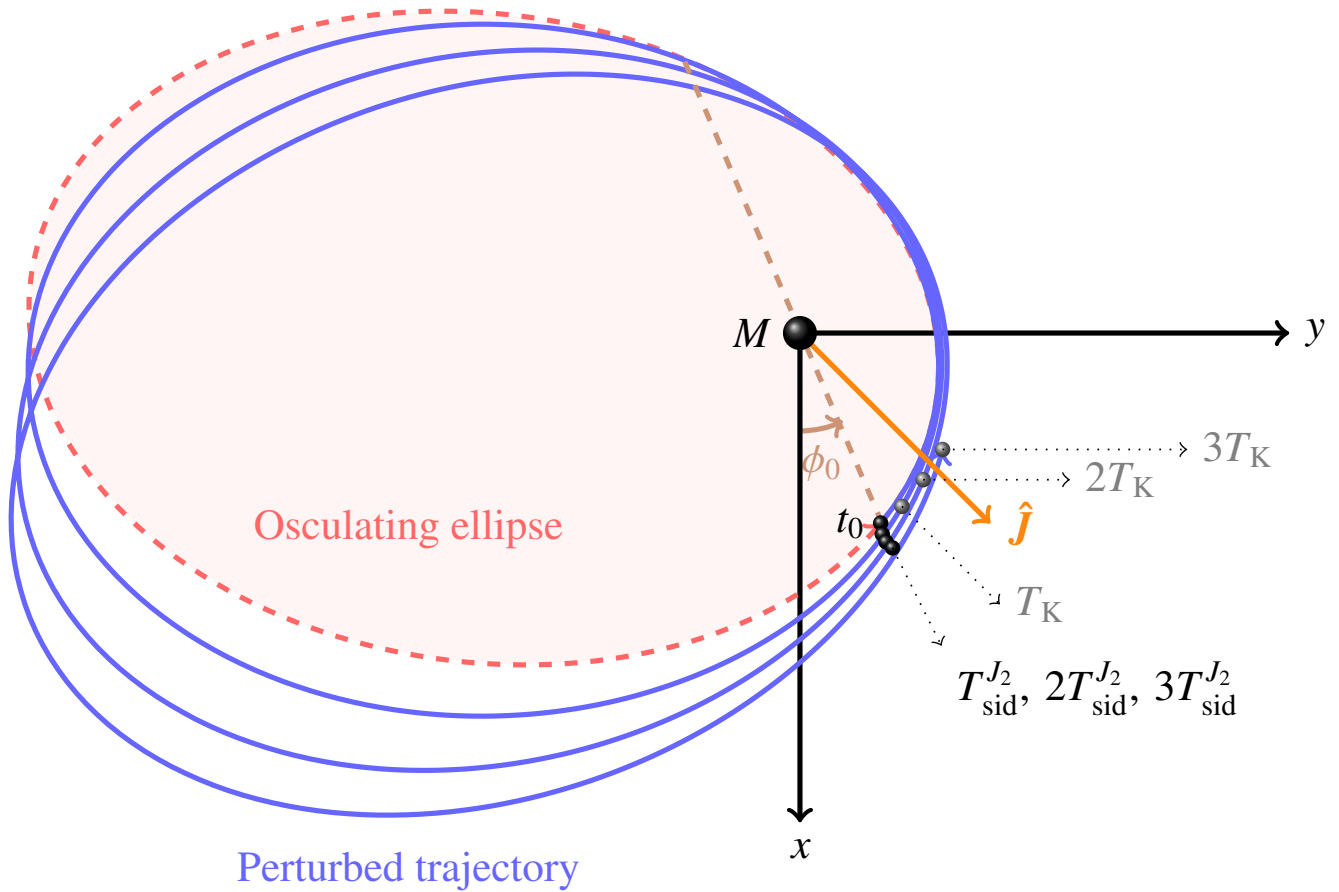


Figure 16. Projections of the perturbed J_2 trajectory (continuous blue curve) and of its osculating Keplerian ellipse (dashed red curve) in the reference plane $\{x, y\}$ at the initial instant of time t_0 characterized by the generic initial conditions $e = 0.7$, $I = 30^\circ$, $\Omega = 45^\circ$, $\omega = 50^\circ$, $f_0 = 285^\circ$. The orientation of the spin axis \hat{J} of the central body, whose projection in the fundamental plane is depicted as well, is set by $\alpha_J = 45^\circ$, $\delta_J = 60^\circ$. In this example, I , Ω , ω and η undergo the known Newtonian shifts due to the quadrupole mass moment J_2 of the primary (Iorio 2017); their magnitudes are suitably rescaled for better visualizing their effect. The positions on the perturbed trajectory after one, two and three Keplerian periods T_K are marked as well. At each orbit, the passages at the generic fixed dashed brown line characterized by ϕ_0 occur always earlier than in the Keplerian case by the amount given by the sum of Equation (86) and Equation (113). It is so because, for the given values of the spin and orbital parameters, $\Delta T_{\text{dra}}^{J_2} + \Delta T_{\text{sid II}}^{J_2} < 0$, as per Equation (86) and Equation (113).

$$+2e^2 \cos^3(l_0 - \varpi)] - 3 \cos(2l_0 - 2\alpha_J) \left\{ (2 + 3e^2) \cos 2\delta_J + 2[1 + e \cos(l_0 - \varpi)]^3 \right\}. \quad (115)$$

In the limit $e \rightarrow 0$, Equation (115) agrees with Equation (114) calculated for $I = 0$.

Figure 16 confirms the analytical results of Equation (86) and Equation (113). Indeed, over three orbital revolutions, the projection of a generic J_2 -perturbed orbit in the fundamental plane $\{x, y\}$ crosses a fixed direction in the latter set by a certain value ϕ_0 always after a time interval equal to $T_{\text{sid}}^{J_2} = T_{\text{dra}}^{J_2} + \Delta T_{\text{sid II}}^{J_2}$ after each orbit. For the particular choice of the primary's spin and the orbital parameters used in the picture, $T_{\text{sid}}^{J_2}$ turns out to be shorter than T_K , in agreement with Equation (86) and Equation (113).

Furthermore, Figure 17 plots the final part of the time series of the cosine of the angle ϕ , normalized to its initial value $\cos \phi_0$, versus time t , in units of T_K , for a numerically integrated fictitious test particle with and without Equation (34) starting from the same generic initial position. It can be seen that it comes back to the same position on the fixed direction chosen in the reference plane, i.e. it is $\cos \phi / \cos \phi_0 = +1$ again, just after $T_{\text{sid}}^{J_2} = T_{\text{dra}}^{J_2} + \Delta T_{\text{sid II}}^{J_2}$ differing from T_K by a (positive) amount in agreement with Equation (86) and Equation (113) for the particular choice of the generic values of the spin and the orbital parameters adopted in the numerical integrations.

6. Some numerical evaluations

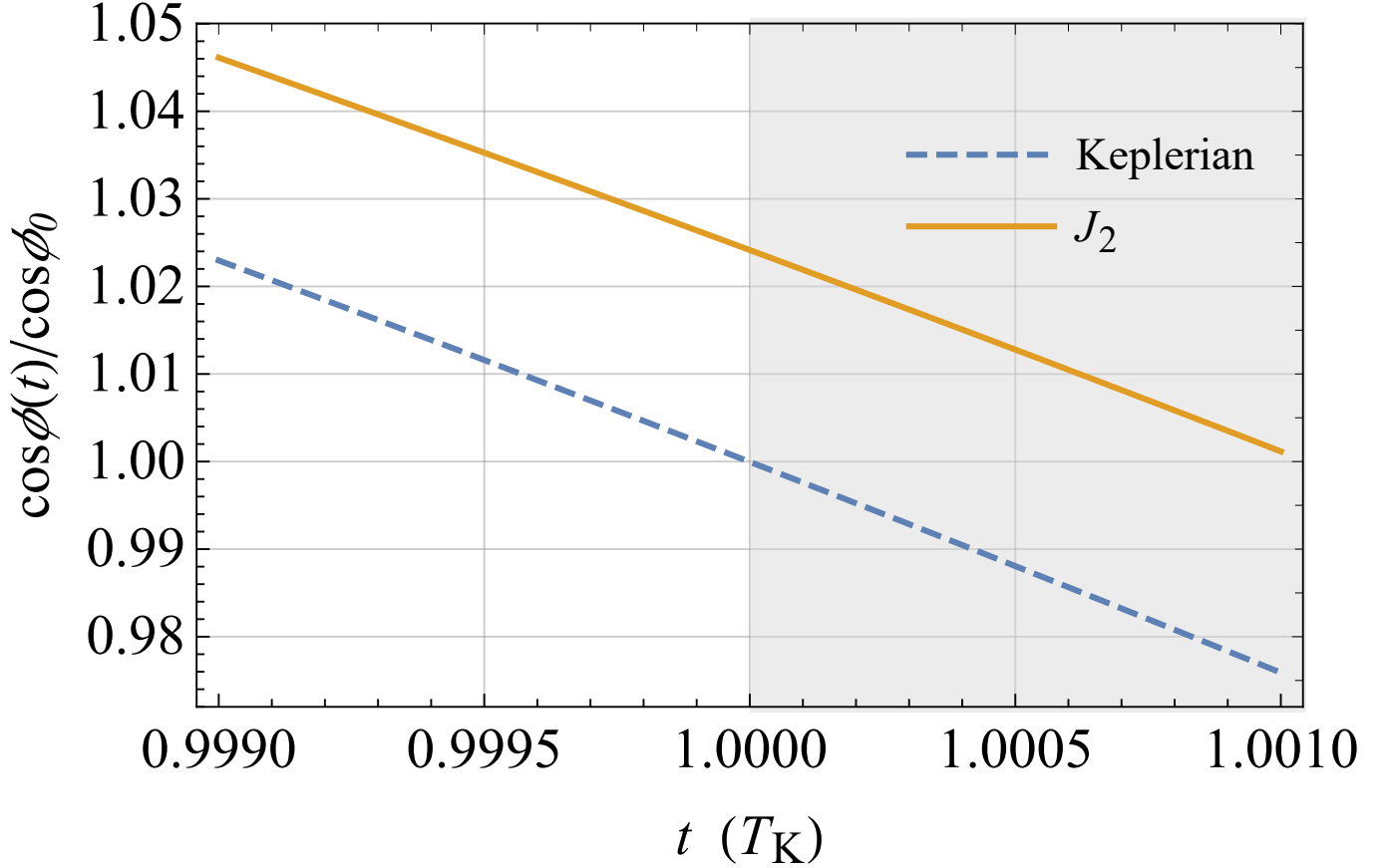


Figure 17. Plot of the numerically produced time series of the cosine $\cos \phi(t)$ of the azimuthal angle $\phi(t)$ normalized to its initial value $\cos \phi_0$ versus time t , in units of T_K , obtained by integrating the equations of motion of a fictitious test particle with (continuous orange curve) and without (dashed azure curve) the J_2 acceleration of Equation (34) for an elliptical ($e = 0.665$) orbit arbitrarily oriented in space ($I = 40^\circ$, $\Omega = 45^\circ$, $\omega = 50^\circ$) starting from, say, the ascending node ϱ ($f_0 = -\omega + 360^\circ$); the semimajor axis is $a = 6R_e$. The physical parameters of the Earth are adopted, apart from the spin axis position set by $\alpha_J = 45^\circ$, $\delta_J = 60^\circ$. The J_2 acceleration is suitably rescaled in such a way that $|\Delta T_{\text{sid}}^{J_2}|/T_K = 0.001$. The time needed to $\cos \phi(t)$ to assume again its initial value $\cos \phi_0$ is longer than in the Keplerian case by the amount $\Delta T_{\text{sid}}^{J_2} = +0.001T_K$, shown by the shaded area, in agreement with the sum of Equation (86) and Equation (113).

The accuracy in measuring the orbital period of several transiting exoplanets (Haswell 2010) is nowadays at the

$$\sigma_T \simeq 10^{-7} - 10^{-8} \text{ d} \simeq 9 \times 10^{-3} - 10^{-4} \text{ s}, \quad (116)$$

level¹¹

Even better accuracies are available for other classes of objects; suffice it to say that the period of WD1032 + 011 b, an inflated brown dwarf in an old eclipsing binary with a white dwarf with

$$\nu = 0.11, \quad (117)$$

is known with an uncertainty as small as (Casewell et al. 2020)

$$\sigma_T \simeq 4.5 \times 10^{-10} \text{ d} = 3.8 \times 10^{-5} \text{ s}. \quad (118)$$

The relevant orbital and physical parameters of WD1032 + 011 b are (Casewell et al. 2020)

$$M_p/M_\odot = 0.0665 \pm 0.0061 \quad (119)$$

¹¹ See <https://exoplanet.eu/home/> and <https://exoplanetarchive.ipac.caltech.edu/>.

$$M_s/M_\odot = 0.4502 \pm 0.0500 \quad (120)$$

$$a/R_\odot = 0.6854 \pm 0.0244, \quad (121)$$

where p and s designate the planet and the star, respectively; M_\odot and R_\odot are the mass and the radius of the Sun, respectively.

By assuming that the measured orbital period is the sidereal¹² one, Equation (78), calculated with Equations (119)–(121), yields

$$\Delta T_{\text{dra}}^{1\text{pN}} = \Delta T_{\text{sid}}^{1\text{pN}} = 0.07 \pm 0.004 \text{ s}. \quad (122)$$

Equation (118) shows that, in principle, the 1pN gravitoelectric correction to the Keplerian orbital period, given by Equation (122), falls within the measurability regime. On the other hand, any excessive optimism should be tempered since the Keplerian term should be finally subtracted from the measured period in order to extract the 1pN component. This implies that the values of the parameters entering the former one should be known to a sufficiently high level of accuracy, which is not yet the case. Indeed, from the errors in Equations (119)–(121), one can calculate that the resulting uncertainty in the Keplerian period is as large as

$$\sigma_{T_K} \simeq 572 \text{ s}. \quad (123)$$

An evaluation of the other pK corrections is not possible since they depend on \mathbf{J} , J_2 and the mutual spin–orbit orientation about which no information is provided by Casewell et al. (2020).

The importance of the issue of the mismodeling in the Keplerian period can be clearly understood in the case of the double pulsar PSR J0737–3039 (Burgay et al. 2003; Lyne et al. 2004), characterized by

$$\nu = 0.2497, \quad (124)$$

and whose (anomalous¹³) orbital period is measured with an accuracy as good as (Kramer et al. 2006)

$$\sigma_T = 5 \times 10^{-11} \text{ d} \simeq 4.32 \times 10^{-6} \text{ s}. \quad (125)$$

In principle, the exquisite accuracy of Equation (125) would allow for an accurate determination of the 1pN gravitoelectric correction to the anomalous period of PSR J0737–3039. Indeed, according to Equation (60), it nominally ranges from

$$0.27 \text{ s} \lesssim \Delta T_{\text{ano}}^{1\text{pN}} \lesssim 0.40 \text{ s}, \quad (126)$$

depending on f_0 . Unfortunately, the uncertainty in the Keplerian period, calculated by propagating the errors in the relevant parameters entering it (Kramer et al. 2006), turns out to be¹⁴

$$\sigma_{T_K} \simeq 9 \text{ s}. \quad (127)$$

Should it be possible to measure for the same system at least two of the three characteristic orbital periods independently, their common Keplerian component would be automatically canceled by forming their difference.

7. Summary and conclusions

It was shown that post–Keplerian accelerations perturbing a two–body gravitationally bound system, like those arising from the oblateness of the central body to the Newtonian level and from the post–Newtonian gravitoelectromagnetic mass and spin–dependent components of its external gravitational potential, breaks the degeneracy between the otherwise coincident anomalous, draconitic and sidereal orbital periods.

The resulting corrections to the Keplerian orbital period are generally different for the aforementioned characteristic timescales. The sidereal period still coincides with the draconitic one when the 1pN gravitoelectric acceleration is taken into account, being both different from the anomalous period. The 1pN gravitomagnetic LT acceleration leaves the anomalous period unaffected with respect to the Keplerian case, while it modifies differently the draconitic and the sidereal periods. Finally, the oblateness of the central body alters all three orbital periods in different ways from each other. In general, all the non–vanishing corrections to the Keplerian orbital period depend on the true anomaly at epoch.

¹² A circular orbit is assumed for WD1032 + 011 b (Casewell et al. 2020).

¹³ A. Possenti, personal communication, May 2024.

¹⁴ Incidentally, the difference between the measured orbital period and the Keplerian one is not statistically significant since it can be calculated to be as small as 1.9 s.

The resulting analytical expressions are completely general since they hold for arbitrary values of the orbital eccentricity and inclination. Furthermore, they are valid also for generic orientations of the primary's symmetry axis in space.

For the transiting brown dwarf WD1032 + 011 b ($\nu = 0.11$), the predicted 1pN gravitoelectric correction to the (sidereal) orbital period amounts to 0.07 s, while the current uncertainty in measuring it is as small as $\approx 10^{-5}$ s, and the mismodeling in the Keplerian part is as large as 572 s. For the double pulsar PSR J0737–3039 ($\nu = 0.2497$), the 1pN gravitoelectric correction to the anomalistic period, which is the measured one for this astrophysical system, is as large as a few tenths of a second; despite the experimental accuracy in measuring the apsidal period is $\approx 10^{-6}$ s, the present-day uncertainty in the calculated value of the Keplerian component is still too large, amounting to about 9 s. If it were possible to measure at least two of the three characteristic orbital timescales independently for the same system, the difference between them would allow the Keplerian term to be canceled a priori.

Data availability

No new data were generated or analysed in support of this research.

Conflict of interest statement

I declare no conflicts of interest.

References

- F. C. Adams and G. Laughlin. Effects of Secular Interactions in Extrasolar Planetary Systems. *Astrophys. J.*, 649:992–1003, 2006a. <https://doi.org/10.1086/506142>.
- F. C. Adams and G. Laughlin. Long-Term Evolution of Close Planets Including the Effects of Secular Interactions. *Astrophys. J.*, 649:1004–1009, 2006b. <https://doi.org/10.1086/506145>.
- F. C. Adams and G. Laughlin. Relativistic Effects in Extrasolar Planetary Systems. *Int. J. Mod. Phys. D*, 15:2133–2140, 2006c. <https://doi.org/10.1142/S0218271806009479>.
- V. M. Amelin. Determination of the Quasi-Nodal Period of the Satellite 1960 ϵ 3 from Simultaneous Visual Tracking Data. In J. Kovalevsky, editor, *Trajectories of Artificial Celestial Bodies as Determined from Observations/Trajectoires des Corps Celestes Artificiels Déterminées D'après les Observations*, pages 15–18. Springer, 1966. https://doi.org/10.1007/978-3-642-49326-3_3.
- G. Antoniciello, L. Borsato, G. Lacedelli, et al. Detecting general relativistic orbital precession in transiting hot Jupiters. *Mon. Not. Roy. Astron. Soc.*, 505:1567–1574, 2021. <https://doi.org/10.1093/mnras/stab1336>.
- B. M. Barker and R. F. O'Connell. Gravitational two-body problem with arbitrary masses, spins, and quadrupole moments. *Phys. Rev. D*, 12:329–335, 1975. <https://doi.org/10.1103/PhysRevD.12.329>.
- B. Bertotti, P. Farinella, and D. Vokrouhlický. *Physics of the Solar System*. Kluwer, 2003. <https://doi.org/10.1007/978-94-010-0233-2>.
- L. Blanchet, G. Hébrard, and F. Larroutourou. Detecting the general relativistic orbital precession of the exoplanet HD 80606b. *Astron. Astrophys.*, 628:A80, 2019. <https://doi.org/10.1051/0004-6361/201935705>.
- R. A. Broucke and P. J. Cefola. On the Equinoctial Orbit Elements. *Celest. Mech. Dyn. Astr.*, 5:303–310, 1972. <https://doi.org/10.1007/BF01228432>.
- D. Brouwer and G. M. Clemence. *Methods of Celestial Mechanics*. Academic Press, 1961.
- V. A. Brumberg. *Essential Relativistic Celestial Mechanics*. Adam Hilger, 1991.
- M. Burgay, N. D'Amico, A. Possenti, et al. An increased estimate of the merger rate of double neutron stars from observations of a highly relativistic system. *Nature*, 426:531–533, 2003. <https://doi.org/10.1038/nature02124>.
- M. Capderou. *Satellites: Orbits and missions*. Springer, 2005.
- S. L. Casewell, C. Belardi, S. G. Parsons, et al. WD1032 + 011, an inflated brown dwarf in an old eclipsing binary with a white dwarf. *Mon. Not. Roy. Astron. Soc.*, 497:3571–3580, 2020. <https://doi.org/10.1093/mnras/staa1608>.
- C. Damiani and A. F. Lanza. Prospecting transit duration variations in extrasolar planetary systems. *Astron. Astrophys.*, 535:A116, 2011. <https://doi.org/10.1051/0004-6361/201117207>.
- T. Damour and N. Deruelle. General relativistic celestial mechanics of binary systems. I. The post-Newtonian motion. *Ann. Inst. Henri Poincaré Phys. Théor.*, 43:107–132, 1985.
- T. Damour, M. Soffel, and C. Xu. General-relativistic celestial mechanics. IV. Theory of satellite motion. *Phys. Rev. D*, 49:618–635, 1994. <https://doi.org/10.1103/PhysRevD.49.618>.
- H. J. Deeg and J. A. Belmonte. *Handbook of Exoplanets*. Springer, 2018. <https://doi.org/10.1007/978-3-319-55333-7>.
- V. A. Egorov. Definition of the True Anomaly in Perturbed Motion. *Sov. Astron.*, 2:147–149, 1958.
- M. T. Eibe, L. Cuesta, A. Ullán, A. Pérez-Verde, and J. Navas. Analysis of variations in transit time and transit duration in WASP-3. Evidence of secular perturbations reconsidered. *Mon. Not. Roy. Astron. Soc.*, 423:1381–1389, 2012. <https://doi.org/10.1111/j.1365-2966.2012.20962.x>.
- A. Fukui, N. Narita, P. J. Tristram, et al. Measurements of Transit Timing Variations for WASP-5b. *Publ. Astron. Soc. Pac.*, 63:287–300, 2011.
- H. Goldstein. *Classical Mechanics. Second Edition*. Addison Wesley, 1980.
- X. Gou, X. Pan, and L. Wang. General Relativity Testing in Exoplanetary Systems. *IOP Conf. Ser.: Earth Environ. Sci.*, 658:012051, 2021. <https://doi.org/10.1088/1755-1315/658/1/012051>.
- C. A. Haswell. *Transiting Exoplanets*. Cambridge University Press, 2010.
- C. Huang, J. C. Ries, B. D. Tapley, and M. M. Watkins. Relativistic effects for near-Earth satellite orbit determination. *Celest. Mech. Dyn. Astr.*, 48:167–185, 1990. <https://doi.org/10.1007/BF00049512>.
- L. Iorio. Are we far from testing general relativity with the transiting extrasolar planet HD 209458b “Osiris”? *New Astron.*, 11:490–494, 2006. <https://doi.org/10.1016/j.newast.2005.12.001>.

- L. Iorio. Classical and relativistic node precessional effects in WASP-33b and perspectives for detecting them. *Astrophys. Space Sci.*, 331:485–496, 2011a. <https://doi.org/10.1007/s10509-010-0468-x>.
- L. Iorio. Classical and relativistic long-term time variations of some observables for transiting exoplanets. *Mon. Not. Roy. Astron. Soc.*, 411:167–183, 2011b. <https://doi.org/10.1111/j.1365-2966.2010.17669.x>.
- L. Iorio. Post-Keplerian corrections to the orbital periods of a two-body system and their measurability. *Mon. Not. Roy. Astron. Soc.*, 460:2445–2452, 2016. <https://doi.org/10.1093/mnras/stw1155>.
- L. Iorio. Post-Keplerian perturbations of the orbital time shift in binary pulsars: an analytical formulation with applications to the galactic center. *Eur. Phys. J. C*, 77:439, 2017. <https://doi.org/10.1140/epjc/s10052-017-5008-1>.
- L. Iorio and M. L. Ruggiero. Constraining the Kehagias–Sfetsos Solution of the Hořava–Lifshitz Modified Gravity with Extrasolar Planets. *The Open Astronomy Journal*, 3:167–171, 2010. <https://doi.org/10.2174/1874381101003010167>.
- A. Jordán and G. Á. Bakos. Observability of the General Relativistic Precession of Periastra in Exoplanets. *Astrophys. J.*, 685:543–552, 2008. <https://doi.org/10.1086/590549>.
- A. Jordán and G. Á. Bakos. Observability of the General Relativistic Precession of Periastra in Exoplanets. In F. Pont, D. Sasselov, and M. Holman, editors, *Transiting Planets. Proceedings IAU Symposium No. 253*, volume 253 of *Proceedings of the International Astronomical Union Symposia and Colloquia*, pages 492–495. Cambridge University Press, 2009. <https://doi.org/10.1017/S1743921308027026>.
- S. R. Kane, J. Horner, and K. von Braun. Cyclic Transit Probabilities of Long-period Eccentric Planets due to Periastron Precession. *Astrophys. J.*, 757:105, 2012. <https://doi.org/10.1088/0004-637X/757/1/105>.
- T. V. Kassimenko. Evaluation of the Satellite Period on the Base of Simultaneous Visual Tracking from Two Given Stations. In J. Kovalevsky, editor, *Trajectories of Artificial Celestial Bodies as Determined from Observations/Trajectoires des Corps Celestes Artificiels Déterminées D'après les Observations*, pages 19–22. Springer, 1966. https://doi.org/10.1007/978-3-642-49326-3_4.
- L. E. Kidder. Coalescing binary systems of compact objects to (post)^{5/2}-Newtonian order. V. Spin effects. *Phys. Rev. D*, 52:821–847, 1995. <https://doi.org/10.1103/PhysRevD.52.821>.
- C. Kitchin. *Exoplanets. Finding, Exploring, and Understanding Alien Worlds*. Springer, 2012. <https://doi.org/10.1007/978-1-4614-0644-0>.
- S. M. Kopeikin, M. Efroimsky, and G. Kaplan. *Relativistic Celestial Mechanics of the Solar System*. Wiley, 2011. <https://doi.org/10.1002/9783527634569>.
- A. Kozak and A. Wojnar. Metric-affine gravity effects on terrestrial exoplanet profiles. *Phys. Rev. D*, 104:084097, 2021. <https://doi.org/10.1103/PhysRevD.104.084097>.
- M. Kramer, I. H. Stairs, R. N. Manchester, et al. Tests of General Relativity from Timing the Double Pulsar. *Science*, 314:97–102, 2006. <https://doi.org/10.1126/science.1132305>.
- L.-S. Li. Parameterized post-Newtonian orbital effects in extrasolar planets. *Astrophys. Space Sci.*, 341:323–330, 2012. <https://doi.org/10.1007/s10509-012-1077-7>.
- D. Lorimer and M. Kramer. *Handbook of Pulsar Astronomy*. Cambridge Observing Handbooks for Research Astronomers. Cambridge University Press, 2005.
- A. G. Lyne, M. Burgay, M. Kramer, et al. A Double-Pulsar System: A Rare Laboratory for Relativistic Gravity and Plasma Physics. *Science*, 303:1153–1157, 2004. <https://doi.org/10.1126/science.1094645>.
- F. Marzari and M. Nagasawa. Influence of general-relativity effects, dynamical tides, and collisions on planet-planet scattering close to the star. *Astron. Astrophys.*, 625:A121, 2019. <https://doi.org/10.1051/0004-6361/201935065>.
- B. Mashhoon. Gravitoelectromagnetism. In J. F. Pascual-Sánchez, L. Floría, A. San Miguel, and F. Vicente, editors, *Reference Frames and Gravitomagnetism*. World Scientific, 2001.
- B. Mashhoon. Gravitoelectromagnetism: A Brief Review. In L. Iorio, editor, *The Measurement of Gravitomagnetism: A Challenging Enterprise*, pages 29–39. Nova Science, 2007.
- J. W. Mason. *Exoplanets. Detection, Formation, Properties, Habitability*. Springer, 2008. <https://doi.org/10.1007/978-3-540-74008-7>.
- V. Mioc and E. Radu. The influence of direct solar radiation pressure on the nodal period of artificial earth satellites. *Astron. Nachr.*, 298:107–110, 1977. <https://doi.org/10.1002/asna.19772980207>.
- V. Mioc and E. Radu. Perturbations in the anomalistic period of artificial satellites caused by the direct solar radiation pressure. *Astron. Nachr.*, 300:313–315, 1979. <https://doi.org/10.1002/asna.19793000610>.
- O. Montenbruck, M. Kirschner, S. D’Amico, and S. Bettadpur. E/I-vector separation for safe switching of the GRACE formation. E/I-Vektor Trennung für den sicheren Wechsel der GRACE Formation. *Aerosp. Sci. Technol.*, 10:628–635, 2006. <https://doi.org/10.1016/j.ast.2006.04.001>.
- C. D. Murray and S. F. Dermott. *Solar System Dynamics*. Cambridge University Press, 1999. <https://doi.org/10.1017/CBO9781139174817>.
- D. E. Ochocimski, T. M. Eneev, and G. P. Taratynova. Bestimmung der Lebensdauer eines künstlichen Erdsatelliten und Untersuchung der säkularen Störungen seiner Bahn. *Fortschritte der Phys.*, 7:34–54, 1959. <https://doi.org/10.1002/prop.19590071404>.
- A. Pál and B. Kocsis. Periastron precession measurements in transiting extrasolar planetary systems at the level of general relativity. *Mon. Not. Roy. Astron. Soc.*, 389:191–198, 2008. <https://doi.org/10.1111/j.1365-2966.2008.13512.x>.
- M. Perryman. *The Exoplanet Handbook. Second edition*. Cambridge University Press, 2018.
- G. Petit and B. Luzum, editors. *IERS Conventions (2010)*, volume 36 of *IERS Technical Note*. Verlag des Bundesamts für Kartographie und Geodäsie, Frankfurt am Main, 2010.
- E. Poisson and C. M. Will. *Gravity. Newtonian, Post-Newtonian, Relativistic*. Cambridge University Press, 2014. <https://doi.org/10.1017/CBO9781139507486>.
- D. Ragozzine and A. S. Wolf. Probing the Interiors of very Hot Jupiters Using Transit Light Curves. *Astrophys. J.*, 698:1778–1794, 2009. <https://doi.org/10.1088/0004-637X/698/2/1778>.
- A. E. Roy. *Orbital Motion. Fourth Edition*. IOP Publishing, 2005.
- M. L. Ruggiero and L. Iorio. Probing a r^{-n} modification of the Newtonian potential with exoplanets. *J. Cosmol. Astropart. Phys.*, 2020:042, 2020. <https://doi.org/10.1088/1475-7516/2020/06/042>.
- S. Seager. *Exoplanets*. University of Arizona Press, 2011.
- I. I. Shevchenko. *The Lidov-Kozai Effect-Applications in Exoplanet Research and Dynamical Astronomy*, volume 441 of *Astrophysics and Space Science Library*. Springer, 2017. <https://doi.org/10.1007/978-3-319-43522-0>.
- M. H. Soffel. *Relativity in Astrometry, Celestial Mechanics and Geodesy*. Springer, 1989. <https://doi.org/10.1007/978-3-642-73406-9>.
- M. H. Soffel and W.-B. Han. *Applied General Relativity*. Astronomy and Astrophysics Library. Springer, 2019. <https://doi.org/10.1007/978-3-030-19673-8>.
- L. Taff. *Celestial Mechanics: A Computational Guide for the Practitioner*. Wiley, 1985.
- G. P. Taratynova. Über die Bewegung von künstlichen Satelliten im nicht-zentralen Schwerefeld der Erde unter Berücksichtigung des Luftwiderstandes. *Fortschritte der Phys.*, 7:55–64, 1959. <https://doi.org/10.1002/prop.19590071405>.

- M. Vargas dos Santos and D. F. Mota. Extrasolar planets as a probe of modified gravity. *Phys. Lett. B*, 769:485–490, 2017. <https://doi.org/10.1016/j.physletb.2017.04.030>.
- C. M. Will. The Confrontation between General Relativity and Experiment. *Living Rev. Relativ.*, 17:4, 2014. <https://doi.org/10.12942/lrr-2014-4>.
- C. M. Will. *Theory and Experiment in Gravitational Physics. Second edition*. Cambridge University Press, 2018. <https://doi.org/10.1017/9781316338612>.
- C. M. Will and N. Yunes. *Is Einstein still right?* Oxford University Press, 2020.
- Y. Xie and X.-M. Deng. On the (im)possibility of testing new physics in exoplanets using transit timing variations: deviation from inverse-square law of gravity. *Mon. Not. Roy. Astron. Soc.*, 438:1832–1838, 2014. <https://doi.org/10.1093/mnras/stt2325>.
- S.-S. Zhao and Y. Xie. Parametrized post-Newtonian secular transit timing variations for exoplanets. *Res. Astron. Astrophys.*, 13:1231-1239, 2013. <https://doi.org/10.1088/1674-4527/13/10/011>.
- I. D. Zhongolovich. Certain Formulas Related to the Motion of a Material Point Within the Gravitational Field of an Ellipsoid of Revolution. *Byul. Inst. Teor. Astron.*, 7:521–536, 1960.
- I. D. Zhongolovich. On the Use of the Results Obtained from Synchronous Observations of the Artificial Satellites of the Earth from the INTEROBS Programme for Scientific Purposes. In J. Kovalevsky, editor, *Trajectories of Artificial Celestial Bodies as Determined from Observations/Trajectoires des Corps Celestes Artificiels Déterminées D'après les Observations*, pages 1–5. Springer, 1966. https://doi.org/10.1007/978-3-642-49326-3_1.